

Ligands

A Novel Pentadentate Redox-Active Ligand and Its Iron(III) Complexes: Electronic Structures and O₂ ReactivityRamona Metzinger,^[a] Serhiy Demeshko,^[b] and Christian Limberg*^[a]

Abstract: A novel redox-active ligand, H₄^{Ph₂S^LAP} (**1**) which was designed to be potentially pentadentate with an O,N,S,N,O donor set is described. Treatment of **1** with two equivalents of potassium hydride gave access to octametallallic precursor complex [H₂^{Ph₂S^LAP}K₂(thf)₄] (**2**), which reacted with FeCl₃ to yield iron(III) complex [H₂^{Ph₂S^LAP}FeCl] (**3**). Employing Fe[N(SiMe₃)₂]₃ for a direct reaction with **1** led to ligand rearrangement through C–S bond cleavage and thiolate formation, finally yielding [HL^{AP}Fe] (**5**). Upon exposure to O₂, **3** and **5** are oxidized through formal hydrogen-atom abstraction from the ligand NH units to form [^{Ph₂S^LSQ}FeCl] (**4**) and [L^{SQ}Fe] (**6**) featuring two or one coordinated iminosemi-

quinone moieties, respectively. Mössbauer measurements demonstrated that the iron centers remain in their +III oxidation states. Compounds **3** and **5** were tested with respect to their potential as models for the catechol dioxygenase. Thus, they were treated with 3,5-di-*tert*-butyl-catechol, triethylamine and O₂. It turned out that the iron–catecholate complexes react with O₂ in dichloromethane at ambient conditions through C–C bond cleavage mainly forming extradiol cleavage products. Intradiol products are only side products and quinone formation becomes negligible. This observation has been rationalized by a dissociation of two donor functions upon coordination of the catecholate.

Introduction

The redox conversion of small substrates often requires multi-electron processes. Metals found in the active site of enzymes, like iron, nickel, or copper, typically mediate only one-electron redox events, but nature circumvents this issue by storage of oxidizing or reducing equivalents in nearby cofactors, such as iron–sulfur clusters, or directly in redox-active ligands surrounding the metal centers, like for instance in galactose oxidase^[1] or in the iron-containing ribonucleotide reductase,^[2] where O₂ activation at the metal center concomitantly leads to a tyrosyl radical.

The redox activity of certain ligand classes has been recognized already some time ago. However, during the last 15 years, many novel and exciting examples have been revealed^[3] and the “non-innocent” behavior of ligands became increasingly recognized.^[4] The term “non-innocence” was introduced to emphasize that redox-active ligands bring about an uncertainty in oxidation-state assignment at the metals to which they coordinate. In recent years, redox-active ligands have been utilized more and more for the conversion/activation of small substrates, partly in a bio-inspired approach.^[5]

A significant amount of research on redox-active ligands is concerned with those containing phenolate moieties, partly owing to their synthetic versatility. Interesting functional systems were obtained when the phenolic function was coupled to an amido group in the *ortho* position.^[6]

In the past, we have employed calixarene and thiacalixarene ligands as supporting ligands for oxovanadium complexes, which proved to be efficient oxidation catalysts.^[7] In none of the systems was a non-innocent behavior observed. More recently, we have investigated thiobisphenolates, which can be regarded as cut-outs of thiacalixarenes, in combination with iron(III) centers.^[8] With the background outlined above, we have now extended this work to develop a pentadentate ligand precursor, *N,N'*-bis(2-hydroxy-3,5-di-*tert*-butylphenyl)-2,2'-diaminodiphenyl-sulfide, H₄^{Ph₂S^LAP} (**1**; Figure 1, AP = aminophenolate). A double deprotonation of **1** leads to [H₂^{Ph₂S^LAP}]²⁻ but concomitantly oxidation reactions can occur through the formal loss of one or even two hydrogen atoms from the N–H functions, ultimately leading to a double semiquinone (SQ), [^{Ph₂S^LSQ}]²⁻, featuring two radical centers (Figure 2).

Such oxidations could occur upon complexation of the ligand to an oxidized metal center or subsequently upon the addition of an oxidant. Hence, an investigation of the behavior

[a] R. Metzinger, Prof. Dr. C. Limberg
Institut für Chemie, Humboldt-Universität zu Berlin
Brook-Taylor-Strasse 2, 12489 Berlin (Germany)
E-mail: christian.limberg@chemie.hu-berlin.de

[b] Dr. S. Demeshko
Georg-August-Universität Göttingen, Institut für Anorganische Chemie
Tammannstrasse 4, 37077 Göttingen (Germany)

Supporting information for this article is available on the WWW under <http://dx.doi.org/10.1002/chem.201304535>.

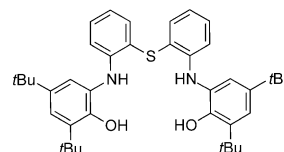


Figure 1. H₄^{Ph₂S^LAP} (**1**) with O,N,S,N,O donor set.

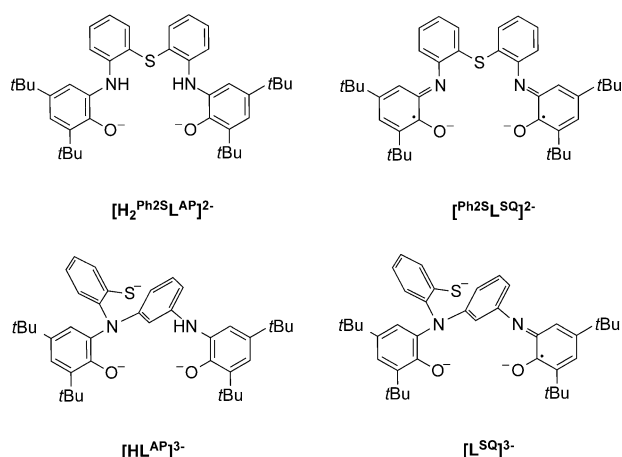


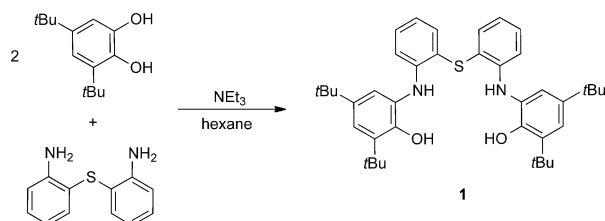
Figure 2. Possible oxidation states of 1 and ligand abbreviations used.

of $[H_2^{Ph2SLAP}]^{2-}$ in the coordination sphere of iron(III) seemed worthwhile. Iron(III) complexes are typically inert in the presence of O_2 and we were interested to examine whether the ligand $[H_2^{Ph2SLAP}]^{2-}$ could change this reactivity. This phenomenon is found in nature. Specifically, the intradiol-cleaving catechol dioxygenase (IDO) is an iron enzyme that contains iron(III) in its resting state, but still is capable of mediating dioxygenation with O_2 through substrate activation, that is, the catechol behaves as a non-innocent ligand and thus is susceptible to attack by O_2 .^[9] The iron(III) center in IDO is surrounded by two phenolates and two histidine ligands, a situation that can be simulated by $[H_2^{Ph2SLAP}]^{2-}$ and hence we intended to also employ this ligand in catechol dioxygenase modelling studies.

Results and Discussion

Synthesis of ligand precursor 1

The compound, $H_4^{Ph2SLAP}$ (1), containing two phenolic and two amine functions as well as a soft thioether donor atom, is accessible in good yields by the reaction of 3,5-di-*tert*-butylcatechol and 2,2'-diaminodiphenyl sulfide in the presence of catalytic amounts of triethylamine at ambient temperatures (Scheme 1). After workup, $H_4^{Ph2SLAP}$ (1) can be obtained as a white solid in 73% yield. Its identity was proved with the aid of NMR and IR spectroscopy, high-resolution electrospray ionization (HR-ESI) mass spectrometry, and CHN elemental analysis. The IR spectrum of 1 shows two intense broad bands at 3482 and 3335 cm^{-1} , attributable to $\nu(OH)$ and $\nu(NH)$ vibrations, re-



Scheme 1. Synthesis of the ligand $H_4^{Ph2SLAP}$ (1).

spectively, which are helpful markers to ascertain the protonation/oxidation state of the ligand after coordination to a metal ion.

A comparison between the metric data of 1 with those of the corresponding ligand systems within the targeted metal complexes was anticipated to provide additional information on the ligands oxidation states, and thus, we were also interested in the solid-state structure of the ligand itself. Suitable crystals of 1 for X-ray diffraction analysis could be obtained by slow evaporation of the volatiles from a dichloromethane/acetonitrile (1:1) solution. The molecular structure of ligand 1 in the solid state is shown in Figure 3. It crystallizes in the centrosymmetric orthorhombic space group *Pccn* with half a molecule

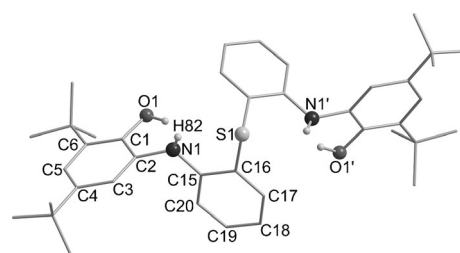
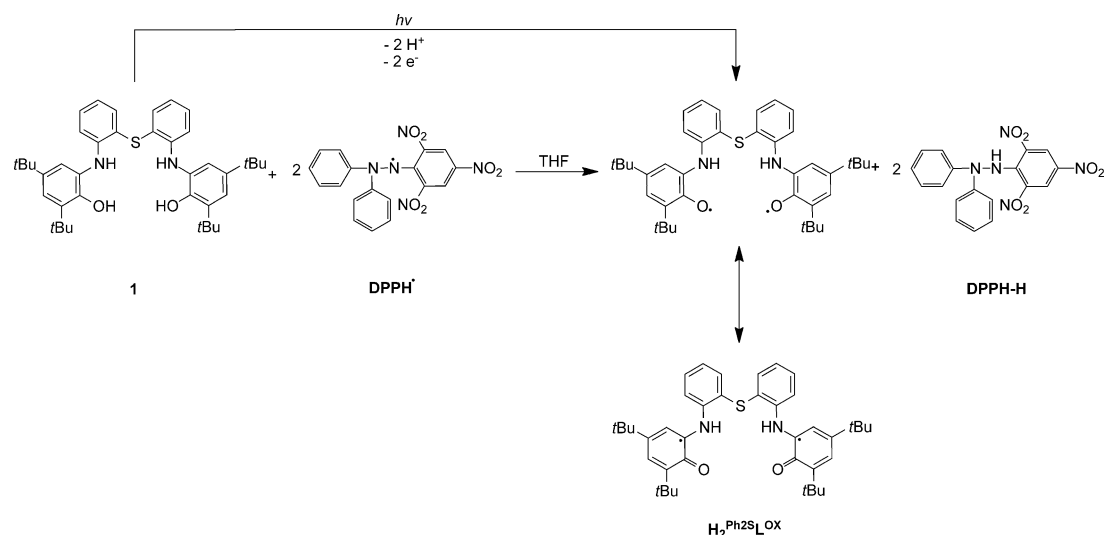


Figure 3. Molecular structure of $H_4^{Ph2SLAP}$ (1), in the solid state. All hydrogen atoms, except for the N–H and O–H protons, have been omitted for clarity. Selected bond length [Å] and angles [°]: C(1)–C(2) 1.395(7), C(2)–C(3) 1.392(8), C(3)–C(4) 1.386(8), C(4)–C(5) 1.382(7), C(5)–C(6) 1.409(7), C(1)–C(6) 1.388(7), C(15)–C(16) 1.414(7), C(16)–C(17) 1.390(8), C(17)–C(18) 1.385(7), C(18)–C(19) 1.392(8), C(19)–C(20) 1.371(8), C(2)–N(1) 1.394(7), C(15)–N(1) 1.444(7), C(1)–O(1) 1.391(6); C(2)–N(1)–H(82) 119.7, C(15)–N(1)–H(82) 108.9.

per asymmetric unit and the inversion center located directly at the sulfur atom, S(1). The C–C distances in the diphenylsulfide backbone [C(15)–C(16) 1.414(7), C(16)–C(17) 1.390(8), C(17)–C(18) 1.385(7), C(18)–C(19) 1.392(8), C(19)–C(20) 1.371(8) Å] as well as in the phenolate moiety [C(1)–C(2) 1.395(7), C(2)–C(3) 1.392(8), C(3)–C(4) 1.386(8), C(4)–C(5) 1.382(7), C(5)–C(6) 1.409(7), C(1)–C(6) 1.388(7) Å] are very similar, thus indicating effective delocalization within the aromatic units. The C(2)–N(1) and C(15)–N(1) distances of 1.394(7) and 1.444(7) Å, respectively, are typical of C–N single bonds; the C(1)–O(1) distance of 1.391(6) Å is typical for aromatic phenols. The C(2)–N(1)–H(82) and C(15)–N(1)–H(82) bond angles, 119.7° and 108.9°, respectively, differ only slightly from the ideal tetrahedral bond angle, thus clearly reflecting the sp^3 hybridization of the nitrogen atoms.

Redox and photochemical behavior of 1

First of all, we were interested to study the redox behavior of 1 itself. To establish the ligand's different oxidation states featuring either a monoradical or biradical constitution, we investigated reactions of 1 with the stable solid radical source, diphenyl picrylhydrazyl (DPPH[•]), in THF at room temperature. Adding two equivalents of DPPH[•] to 1 led to the formation of an orange solution, indicating the generation of the corresponding hydrazine, DPPH-H (2,2-diphenyl-1-picrylhydrazine),



Scheme 2. Formation of $H_2^{Ph25L^{OX}}$ in the reaction of **1** with DPPH $^{\cdot}$ and upon irradiating **1**. Only two mesomeric structures of $H_2^{Ph25L^{OX}}$ are shown.

and concomitant oxidation of **1** to give, $H_2^{Ph25L^{OX}}$ (Scheme 2). Adding excess or only 0.5 equivalents of DPPH $^{\cdot}$ to **1** also resulted in the formation of the ligand in its biradical constitution (in the case of addition of 0.5 equiv, 0.5 equiv of **1** remained unreacted).

The formation of the diradical $H_2^{Ph25L^{OX}}$ has been confirmed by EPR spectroscopy. The EPR spectrum of $H_2^{Ph25L^{OX}}$ in THF at room temperature shows a symmetrical signal with a g value of 2.004, which lies in the typical range for organic radicals. It can be simulated adequately allowing for hyperfine interactions of a one-electron system to one nitrogen and one hydrogen atom in the immediate vicinity (see Figure 4), which may suggest a localization of the electron at the C atom adjacent to the N atom and a coupling to the nearest ring H atom. On the basis of the simulated data, no electron–electron coupling

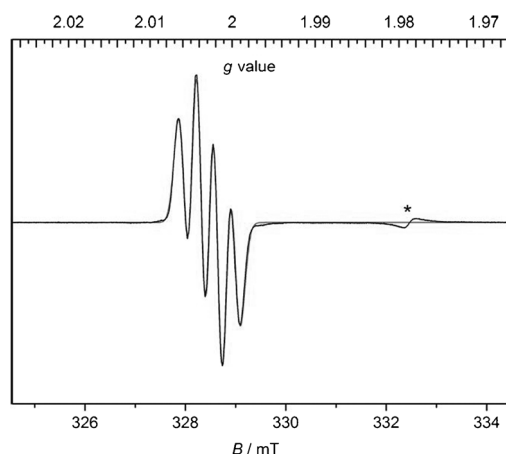
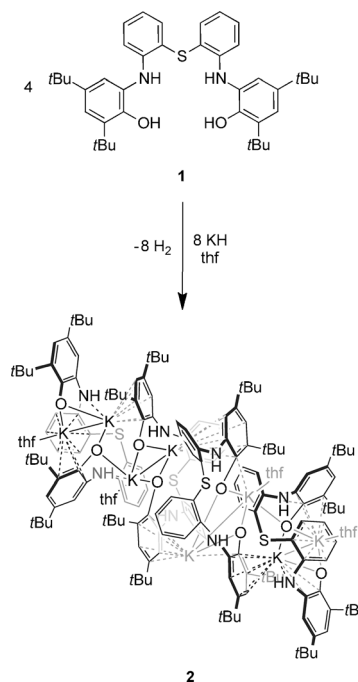


Figure 4. EPR spectrum of a THF solution of the reaction product of **1** in contact with two equivalents of DPPH $^{\cdot}$. The experimental spectrum shows the Cr^{3+}/MgO (*) standard at $g = 1.9796$; the simulated spectrum does not show this feature. The g value was determined to be 2.004; ($A_{H\text{ atom}}$ 10 MHz coupling to the unpaired electron; $A_{N\text{ atom}}$ 9 MHz coupling to the unpaired electron; spectrometer frequency, 9.246 GHz).

seems to be occurring between both radical spins in the oxidized ligand system. Interestingly, irradiation of **1** with a mercury lamp also causes the formation of $H_2^{Ph25L^{OX}}$, as monitored by EPR spectroscopy. Notably, **1** is stable against O_2 both in the solid state and in solution.

Complex synthesis

Addition of 2.2 equivalents KH to a clear colorless solution of **1** in THF leads to the evolution of gas (H_2) and a color change to yellow, both indicative of a successful deprotonation (Scheme 3). After workup, $[H_2^{Ph25L^{AP}}K_2(thf)]_4$ (**2**) was isolated as



Scheme 3. Synthesis of $[H_2^{Ph25L^{AP}}K_2(thf)]_4$ (**2**).

an orange-yellow solid in nearly quantitative yield (98%). Compound **2** is readily soluble in tetrahydrofuran, dichloromethane, acetonitrile, toluene, diethyl ether, and benzene, but almost insoluble in hexane. The IR spectrum of **2** shows a broad band at 3306 cm^{-1} , thus confirming the presence of the -NH groups in **2**. A ^1H NMR spectrum of **2** recorded in $[\text{D}_8]\text{THF}$ also showed characteristics that confirmed the exclusive deprotonation of the phenol units and therefore the formation of $[\text{H}_2^{\text{Ph}_2\text{S}_1\text{L}^{\text{AP}}}]^{2-}$: signals corresponding to OH protons (in case of $\text{H}_4^{\text{Ph}_2\text{S}_1\text{L}^{\text{AP}}}$ (**1**) at 7.34 ppm) had disappeared.

For the two NH protons per ligand, a single resonance was detected at 8.12 ppm (see the Supporting Information). Notably, apparently the thf ligands can be removed under vacuum, as the integrals of the multiplet signals belonging to the protons of coordinated thf molecules decrease with increased drying time prior to the measurement. Obviously, double deprotonation of $\text{H}_4^{\text{Ph}_2\text{S}_1\text{L}^{\text{AP}}}$ is thermodynamically favored: selective removal of one, three, or four protons from the ligand precursor giving its mono-, tri- or tetraanionic forms, respectively, could not be observed.

Crystals of **2** suitable for single-crystal X-ray diffraction could be grown by slow diffusion of hexane into a concentrated THF solution of **2**. It crystallizes in the triclinic centrosymmetric space group, $P\bar{1}$, with half a molecule per asymmetric unit. The structural motif of **2** is complex. It can be considered as an octanuclear potassium complex composed of four ligand anions $[\text{H}_2^{\text{Ph}_2\text{S}_1\text{L}^{\text{AP}}}]^{2-}$, that display extensive K–phenyl π interactions. The NH protons were located in the difference Fourier map, thus supporting the observations in the NMR experiments.

Figure 5 displays the asymmetric unit of compound **2** (for the complete molecular structure, see the Supporting Informa-

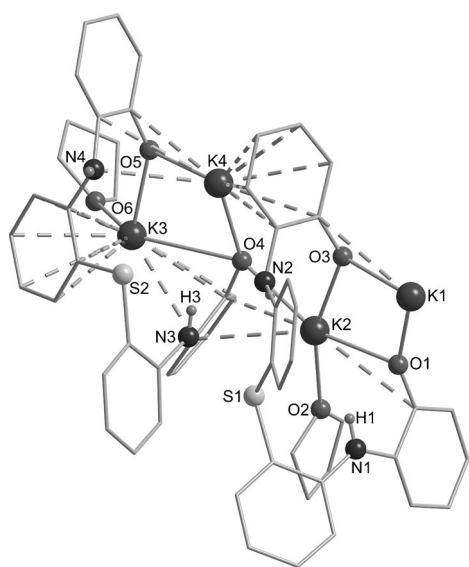


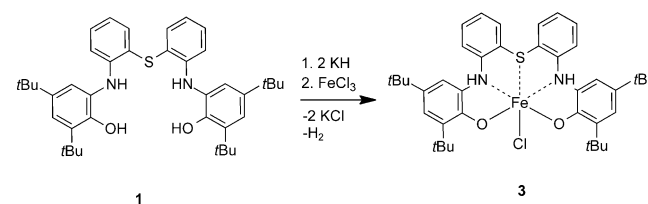
Figure 5. Asymmetric unit of $[\text{H}_2^{\text{Ph}_2\text{S}_1\text{L}^{\text{AP}}}\text{K}_2(\text{thf})_4]$ (**2**). All hydrogen atoms, except for the N–H protons, and all *tert*-butyl groups on the ligand system have been omitted for clarity. Selected bond length [Å]: K(1)⋯K(2) 4.1545(13), K(3)⋯K(4) 3.9131(15), K(1)–O(1) 2.527(3), K(1)–O(3) 2.567(3), K(2)–O(1) 2.612(3), K(2)–O(3) 2.696(3), K(2)–O(2) 2.686(4), K(2)–O(4) 2.753(3), K(2)–N(2) 3.205(4), K(3)–O(4) 3.167(3), K(3)–O(5) 2.531(3), K(3)–O(6) 2.665(3), K(4)–O(4) 2.600(3), K(4)–O(5) 2.601(3), K(4)–N(4) 3.234(4), K(4)–S(2) 3.6360(14), N(1)–H(1) 0.80(5), N(3)–H(3) 0.74(5).

tion). Potassium ions K(2) and K(3) are surrounded by two different ligand moieties. K(4) is surrounded by the donor atoms of only one ligand and the coordination sphere is completed by a thf solvent molecule. K–C interactions are usually considered as relevant up to an arbitrary range of 3.5 Å .^[10a] By using this criterion, K(4) is η^6 -coordinated to the C_6H_4 ring of the backbone belonging to a second ligand as well as η^3 -coordinated to the phenylene ring of the aminophenolate unit. Compound **2** shows close K⋯K contacts, namely K(1)⋯K(2) [4.1545(13) Å] and K(3)⋯K(4) [3.9131(15) Å], which are shorter than those in potassium metal (4.54 Å)^[10b] and much smaller than double the van der Waals radius of potassium ($r_{\text{vdw}} = 2.75\text{ Å}$)^[11].

To explore whether the solid-state structure of **2** is retained upon dissolution, a solution of **2** in THF was investigated by DOSY NMR measurements. These results indicate that **2** is split into $[\text{H}_2^{\text{Ph}_2\text{S}_1\text{L}^{\text{AP}}}\text{K}_2(\text{thf})]$ monomers in solution (see the Supporting Information).

After in situ synthesis of **2** with two equivalents of potassium hydride in dry THF, addition of FeCl_3 to the yellow solution caused a rapid color change to violet. After workup, $[\text{H}_2^{\text{Ph}_2\text{S}_1\text{L}^{\text{AP}}}\text{FeCl}]$ (**3**) was isolated as a black solid in 88% yield. Compound **3** is readily soluble in tetrahydrofuran, dichloromethane, hexane, diethyl ether, benzene, and toluene and moderately soluble in acetonitrile. Attempts to crystallize **3** failed so far, so that its composition and electronic structure had to be elucidated chemically and spectroscopically.

$[\text{IrCl}(\text{PPh}_3)_3]$ is known to form very stable dihydride complexes in the presence of dihydrogen ($[\text{Ir}(\text{H})_2\text{Cl}(\text{PPh}_3)_3]$), which may be utilized to prove dihydrogen formation.^[12] However, the dihydride could not be detected after transferring the gas phase belonging to the reaction of the deprotonated ligand precursor with FeCl_3 into a solution of $[\text{IrCl}(\text{PPh}_3)_3]$ in $[\text{D}_6]$ benzene, while the same procedure applied to the synthesis of **2** did give evidence for dihydrogen generation (through the corresponding signals for the dihydride in the ^1H NMR spectra). Therefore we postulate the formation of **3** with intact NH units as shown in Scheme 4.



Scheme 4. Synthesis of $[\text{H}_2^{\text{Ph}_2\text{S}_1\text{L}^{\text{AP}}}\text{FeCl}]$ (**3**).

Further evidence for the formation of **3** with intact NH units came from IR spectroscopy, which allows one to distinguish between aminophenolate and semiquinonate ligand systems chelated to the metal as the C–O stretching frequency is a sensitive indicator of the ligand oxidation state: the semiquinone ligand usually exhibits strong absorption bands in the range $1420\text{--}1460\text{ cm}^{-1}$, whereas in the IR spectra of phenolate anions, bands at 1580 cm^{-1} of medium intensity and weaker

bands at 1550 and 1520 cm^{-1} can be observed.^[13] The IR spectrum of **3** shows characteristic absorption bands at 1587 and 1521 cm^{-1} , thus indicating clearly the existence of the aminophenolate ligand system $[\text{H}_2^{\text{Ph}_{25}\text{L}^{\text{AP}}}]^{2-}$ in **3**. To gain further insights into the electronic structure, EPR measurements at 77 K were performed for a THF solution of **3**. The spectrum exhibits a g value of 4.26, which is typical for a mononuclear high-spin Fe^{III} ($S=5/2$) complex with the nearest environment being of rhombic symmetry (see the Supporting Information). In addition, Mössbauer measurements of **3**, which provide independent spectroscopic information on the local spin and oxidation state of the iron center, were performed. The spectrum of solid **3** recorded at 80 K is shown in Figure 6. It shows a single quadrupole doublet with an isomer shift of $\delta=0.50 \text{ mm s}^{-1}$ and quadrupole splitting of $\Delta E_{\text{Q}}=1.68 \text{ mm s}^{-1}$. As Fe^{III} centers typically display δ values between 0.4 and 0.6 mm s^{-1} ,^[14] the observed shift underlines the existence of the iron ion in its +III physical oxidation state.

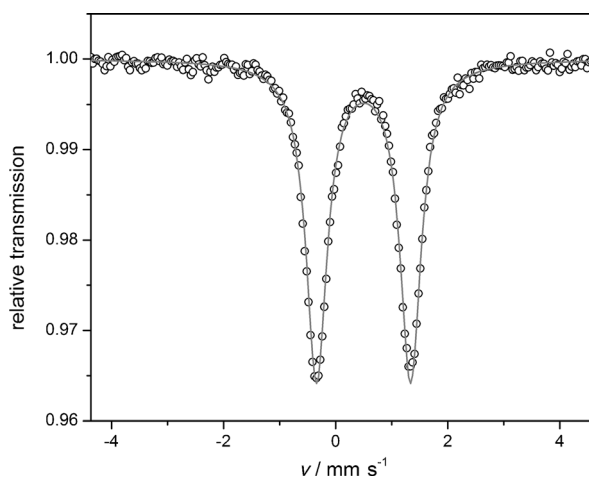


Figure 6. Mössbauer spectrum of solid **3** at 80 K. The following parameters have been fitted to the experimental data points: $\delta=0.50 \text{ mm s}^{-1}$, $\Delta E_{\text{Q}}=1.68 \text{ mm s}^{-1}$, and $\Gamma=0.46 \text{ mm s}^{-1}$.

Complex **3** is very sensitive to O_2 , both in the solid state and in solution. Upon treatment of a solution of **3** in THF with excessive O_2 at -60°C , the violet solution slowly changed its color to green. Repeating this experiment at temperatures ranging from -50°C to 10°C revealed an acceleration of this process with temperature, and performing this experiment at room temperature immediately gave a green solution. In all cases, workup led to a black solid and crystals of the product suitable for single-crystal X-ray diffraction analysis could be obtained by slow evaporation of the volatiles from a concentrated solution in a mixture of acetonitrile and dichloromethane (1:1). Hence, the molecular structure of $[\text{Ph}_{25}\text{L}^{\text{SQ}}\text{FeCl}]$ (**4**), as shown in Figure 7, could be revealed. Complex **4** crystallizes in the monoclinic centrosymmetric space group, $P2_1/c$, with four molecules in the unit cell, and their structures indicate the presence of the diradical, $[\text{Ph}_{25}\text{L}^{\text{SQ}}]^{2-}$ (see Scheme 5).

The Fe^{III} center exhibits a distorted octahedral coordination sphere and is coordinated by the O,N,S,N,O donor set of the

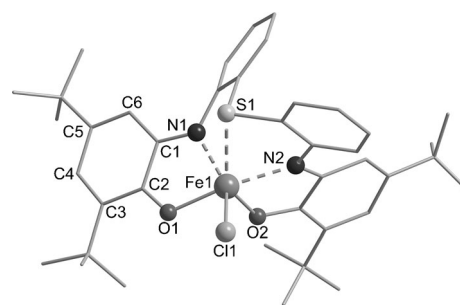
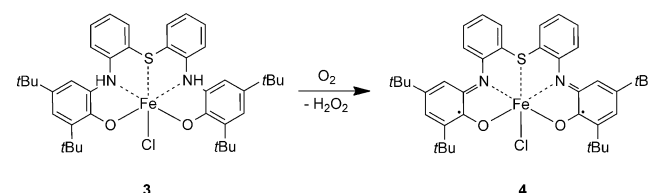


Figure 7. Molecular structure of complex $[\text{Ph}_{25}\text{L}^{\text{SQ}}\text{FeCl}]$ (**4**). Hydrogen atoms are omitted for clarity. Selected bond length/ \AA and angles/ $^\circ$: C(1)–C(2) 1.4518(19), C(2)–C(3) 1.4354(18), C(3)–C(4) 1.3765(19), C(4)–C(5) 1.4366(19), C(5)–C(6) 1.3679(18), C(6)–C(1) 1.4276(18), C(1)–N(1) 1.3451(17), C(13)–N(2) 1.3346(17), C(2)–O(1) 1.2927(16), C(18)–O(2) 1.2886(15), Fe(1)–Cl(1) 2.2753(4), Fe(1)–S(1) 2.6561(4), Fe(1)–N(1) 2.1374(11), Fe(1)–N(2) 2.1026(11), Fe(1)–O(1) 1.9784(9), Fe(1)–O(2) 2.0025(9), O(1)–Fe(1)–S(1) 144.50(3), O(2)–Fe(1)–S(1) 120.23(3), O(1)–Fe(1)–O(2) 88.00(4), O(1)–Fe(1)–N(1) 76.86(4), O(1)–Fe(1)–N(2) 98.58(4), O(2)–Fe(1)–N(1) 164.64(4), O(2)–Fe(1)–N(2) 75.91(4), Cl(1)–Fe(1)–O(2) 91.90(3), Cl(1)–Fe(1)–O(1) 111.14(3).



Scheme 5. Synthesis of $[\text{Ph}_{25}\text{L}^{\text{SQ}}\text{FeCl}]$ (**4**).

pentadentate ligand with the two nitrogen donor atoms, N(1) and N(2), as well as the two oxygen atoms, O(1) and O(2), in the position *cis* to each other. The coordination sphere of the iron center is completed by a chlorido ligand. The C–C distances of the diphenylsulphide backbone range from 1.3840(2) to 1.4104(18) \AA , thus indicating that the conjugation in these phenyl rings is retained. In contrast, the six C–C distances in the *tert*-butyl-substituted rings are different [C(1)–C(2) 1.4518(19) \AA , C(2)–C(3) 1.4354(18) \AA , C(3)–C(4) 1.3765(19) \AA , C(4)–C(5) 1.4366(19) \AA , C(5)–C(6) 1.3679(18) \AA , C(6)–C(1) 1.4276(18) \AA] and display the typical pattern of iminobenzo-semiquinone radicals with three adjacent long bonds flanked by two short bonds and a long bond between them, as one would expect according to Scheme 5. Thus, the *tert*-butyl-substituted rings adopt a quinoid-type structure. Furthermore, the planar coordination geometry around the nitrogen donor atoms, N(1) and N(2), indicate sp^2 hybridization, and thus, a deprotonation of nitrogen atoms, consistent with IR measurements, which gave no evidence for any bands corresponding to $\nu(\text{NH})$ vibrations. Moreover, the bond lengths, C(1)–N(1) and C(13)–N(2) with 1.3451(17) and 1.3346(17) \AA , respectively, clearly show double-bond character in contrast to the C–N bond lengths found in **2** (for example, C(2)–N(1) 1.424(5) \AA). Additionally, the C(2)–O(1) and C(18)–O(2) bond lengths with 1.2927(16) and 1.2886(15) \AA are significantly shorter than typical C–O bonds belonging to aromatic phenols (for example, C(1)–O(1) 1.316(5) \AA in **2**). With 2.2753(4) \AA , the Fe(1)–Cl(1) bond length falls within the typical range for Fe–Cl distances

in six-coordinate iron(III) complexes.^[17] The Fe(1)–S(1) distance in **4** with 2.6561(4) Å fits well to those reported previously for iron thiacalix[4]arene complexes or other iron(III) complexes with thioether ligands.^[8,18]

As mentioned above, vibrational spectroscopy is a valuable method to characterize metal-bound phenolates and semiquinones. The Raman spectrum of complex **3** (Figure 8) shows a prominent peak at 1217 cm⁻¹ arising from the typical phenolate aromatic ring mode (ν_{C-O}). After reaction of **3** with O₂, this band vanished, while new bands were observed and the dominant feature at 1417 cm⁻¹, according to literature, can reasonably be assigned to the symmetric C–O stretching mode of the coordinated semiquinone ligand system in **4**.^[19] Additional modes were observed at 1371, 1359, and 1317 cm⁻¹ corresponding to intraligand C–C bond motions. Oxidation product **4** was further characterized by IR, Mössbauer spectroscopy, and Evans measurements.

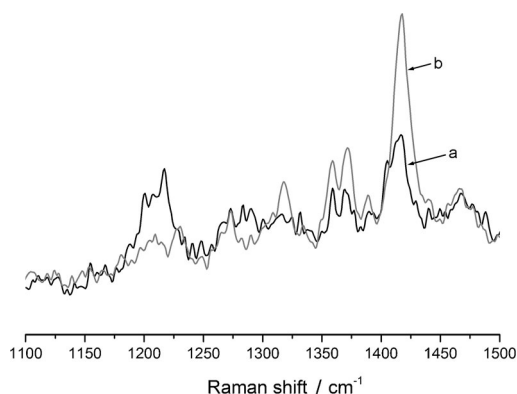


Figure 8. Raman spectra of **3** recorded before (a) and after the reaction with O₂ (b; $\lambda_{\text{ex}} = 1064$ nm, THF, room temperature).

The Mössbauer spectrum of solid **4** at 80 K shows one quadrupole doublet with $\delta = 0.51$ mm s⁻¹ and $\Delta E_Q = 1.16$ mm s⁻¹, thus clearly indicating the presence of high-spin Fe^{III} (see Figure 9). Compared to **3**, the quadrupole splitting is smaller, pointing to a higher symmetry and less distortion in **4**. The observed isomer shift is in excellent agreement with shifts reported for comparable compounds in the literature: Mössbauer spectra of high-spin Fe^{III}-iminosemiquinone complexes exhibit δ values ranging from 0.44 to 0.54 mm s⁻¹.^[20]

The magnetic properties of complex **4** in solution were probed by using the Evans method. The magnetic moment of $\mu_{\text{eff}} = 3.35 \mu_B$ was determined for **4** at room temperature in a [D₃]chloroform solution. The result is in accordance with the spin-only value for three unpaired electrons at one iron center with a total spin quantum number of $S = 3/2$ ($\mu_{\text{so}} = 3.87 \mu_B$) owing to an antiferromagnetic spin coupling between the high-spin iron(III) center and both radical anions of the oxidized ligand.

Having identified the geometric and electronic structure of **4**, it became clear that the oxidation of **3** by O₂ to give **4** occurs through two H atom abstractions (or proton-coupled electron transfers, PCETs), and the formation of H₂O₂ as an im-

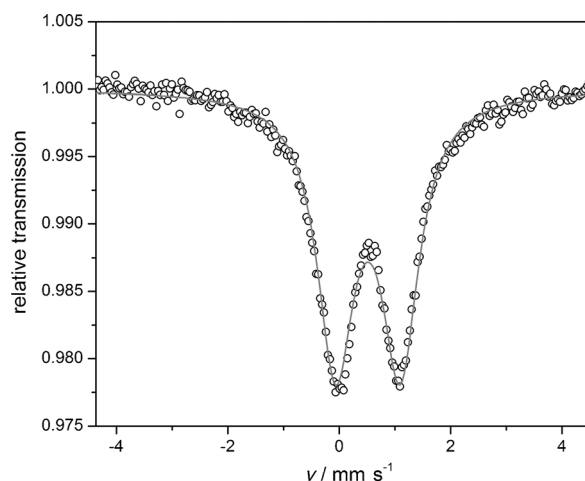


Figure 9. Mössbauer spectrum of solid **4** at 80 K. The following parameters have been fitted to the experimental data points: $\delta = 0.51$ mm s⁻¹, $\Delta E_Q = 1.16$ mm s⁻¹ and $\Gamma = 0.80$ mm s⁻¹.

mediate by-product was conceivable. Hence we tested for hydrogen peroxide according to a literature procedure that uses the titanil sulfate as the reagent. A necessary condition for the successful detection of hydrogen peroxide is of course its stability in the presence of oxidation product **4**. To examine this compatibility, a THF solution of **4** was treated with H₂O₂ and, subsequently, it was added to an aqueous, acidic titanil sulfate solution. After dilution, the UV/Vis spectrum showed a strong absorption with a maximum at 401 nm, which can be attributed to the O₂²⁻ → Ti ligand-to-metal charge transfer, according to the literature (see the Supporting Information).^[15] When a blind experiment using the same procedure but omitting H₂O₂ was conducted, the band was not observed. It may be concluded that **4** does not rapidly decompose H₂O₂. In the next step, the mixture obtained through reaction of **3** with O₂ was added to titanil sulfate. Also, in this case, a UV/Vis spectrum showed a strong absorption band at 385 nm assignable to an O₂²⁻ → Ti ligand-to-metal charge transfer. Furthermore, IR spectroscopic investigations (KBr disc after removal of all volatiles) showed a sharp band at 715 cm⁻¹. The absence of this band in the IR spectra of the Ti peroxo free samples after workup supports that this band may be attributed to a metal–peroxide stretching vibration; according to the literature, the position of the band is typical for titanium–peroxide absorptions.^[16] Hence, these results suggest that indeed the reaction in Scheme 5 proceeds with formation of hydrogen peroxide.

Complementarily, the reaction between **3** and O₂ was followed by UV/Vis spectroscopy. The UV/Vis measurements showed that, during the reaction of **3** with O₂ at room temperature, two new absorption features evolve (Figure 10): the broad band of **3** in the visible region at 844 nm ($\epsilon = 2836$ M⁻¹ cm⁻¹) is shifted hypsochromically by 109 nm to a wavelength of 775 nm ($\epsilon = 3619$ M⁻¹ cm⁻¹) and a new broad absorption at 475 nm ($\epsilon = 2622$ M⁻¹ cm⁻¹) appears. The oxidation reaction is characterized by two quasi-isobestic points at 485 nm and 638 nm. The new absorption feature at 775 nm compares well with absorption spectra reported for related

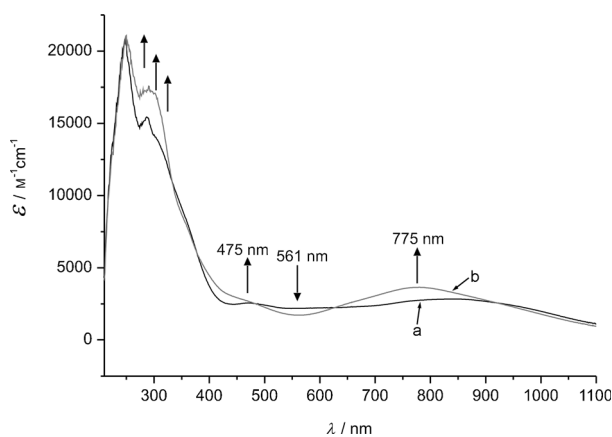
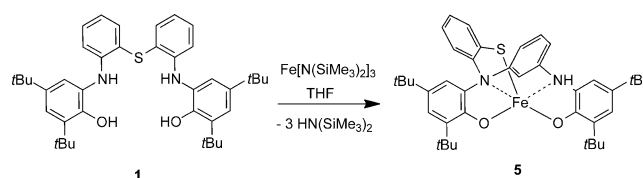


Figure 10. UV/Vis spectra of a solution of **3**, dissolved in THF (0.15 mM) before (a) and 10 min after the reaction with O_2 at room temperature (b).

iminosemiquinone-containing complexes with various metal ions (Co^{3+} , Ni^{2+} , and Cu^{2+}), as well as with a spectrum measured for a "free" iminosemiquinone radical.^[21] These spectral similarities suggest that the transitions observed during the addition of O_2 to **3** are primarily ligand based (intraligand transition). The UV/Vis spectra of **4** is identical to the one recorded directly after exposing a sample of **3** to air, as depicted in Figure 10.

Interestingly, heating complex **3** to $60^\circ C$, directly after its treatment with O_2 , leads to the conversion of initially formed **4** into a new complex in a low-spin state (see the Supporting Information), as monitored by electronic spin resonance measurements: after freezing of such a heated sample to 77 K, its EPR spectrum displays a rhombic low-spin signal ($g_z=2.240$, $g_y=2.061$, $g_x=2.005$); this low-spin component can only be observed after the reaction with O_2 . Heating complex **3** does not lead to the formation of the low-spin species and neither does heating of **4**, that is, the presence of O_2 is essential. We conclude that upon exposure of **3** to O_2 followed by heating, an intermediate species is formed with an iron atom in a strong octahedral ligand field.

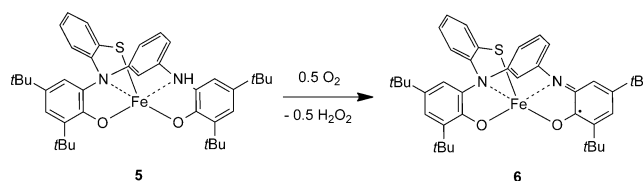
To evaluate the role of the chlorido co-ligand in **3**, an iron(III) precursor with basic ligands that allow for an in situ deprotonation of **1** followed by iron complexation was employed. Treatment of ligand precursor **1** with iron(III)bis(trimethylsilyl)amide in a 1:1 ratio in dry THF caused a rapid color change to an intense purple, indicating a spontaneous complexation of the ligand precursor. Again, generation of H_2 could be excluded with the aid of $[IrCl(PPh_3)_3]$. After workup, IR, EPR, and Mössbauer spectroscopy was used to identify the product as $[HL^{AP}Fe]$ (**5**), which could be isolated as a purple solid in 69% yield (Scheme 6). Formation of **5** can be explained assuming that, first of all, both phenol units and one of the amine functions get deprotonated by the basic silazide ligands so that a structure similar to that of **3** or **4** (disregarding the chlorido ligands) is formed. However, while in these compounds both $Fe\cdots N$ bonds are coordinate bonds, the initial complex formed from **1** and $Fe[N(SiMe_3)_2]_3$ will contain one covalent $Fe-N$ bond that will be significantly shorter, thus caus-



Scheme 6. Product of the reaction of **1** with $Fe[N(SiMe_3)_2]_3$.

ing strain in the structure. It is thus understandable that such a structure should relax through C–S bond cleavage and movement of the respective phenyl residue to the nearby amide function, resulting in coordinating amine and thiolate functions. Cleavage of C–S bonds next to a benzylic position has been observed before, and metal-catalyzed carbon–sulfur bond cleavage reactions are important in synthetic chemistry.^[22] Many of these cleavage reactions occur through radical formation,^[23] but we exclude this mechanism for the formation of **5** by the fact that the reaction is not inhibited by radical scavenger reagents, such as 2,6-dimethylphenol or 2,6-di-*tert*-butyl-4-methylphenol. Compound **5** is readily soluble in tetrahydrofuran, dichloromethane, acetonitrile, hexane, benzene, toluene, and diethyl ether.

The IR spectrum of **5** shows characteristic $\nu(C-O)$ absorption bands at 1582 cm^{-1} and 1523 cm^{-1} , thus clearly indicating coordinating aminophenolate units. Noteworthy is also the occurrence of an absorption band at 3316 cm^{-1} attributable to a $\nu(N-H)$ vibration of the ligand. The EPR spectrum of **5** in a THF matrix at 77 K shows a typical iron(III) high-spin signal ($g'=4.230$ for the $|-1/2\rangle \rightarrow |+1/2\rangle$ transition), reflecting rhombic symmetry of the ligand field (see the Supporting Information). Like **3**, complex **5** is extremely sensitive to O_2 , both in the solid state and in solution, and reacts to give $[L^{SQ}Fe]$ (**6**), as revealed by X-ray diffraction analysis, IR, Mössbauer, and UV/Vis spectroscopy (see Scheme 7). Hence, no $\nu(N-H)$ band



Scheme 7. Synthesis of $[L^{SQ}Fe]$ (**6**).

can be observed in the IR spectrum of **6**, which however, shows a strong band at 1259 cm^{-1} , attributable to a $\nu(C-O)$ stretching vibrations of the phenolate moiety, as well as a strong absorption feature at 1466 cm^{-1} , attributable to the $\nu(C-O)$ mode, as should be expected for the iminosemiquinone–aminophenolate ligand, $[L^{SQ}]^{3-}$.

Slow evaporation of the volatiles from a concentrated solution of **6** in a mixture of dichloromethane and acetonitrile (1:1) led to crystals suitable for single-crystal X-ray diffraction analysis. The structural identification of **6** further corroborates the structure of **5**. Complex **6** crystallizes in the monoclinic centro-

symmetric space group, $P2_1/c$, with four molecules in the unit cell, and its molecular structure is shown in Figure 11. The molecule consists of a single iron center coordinated by one semiquinonate ligand system. The coordination geometry around

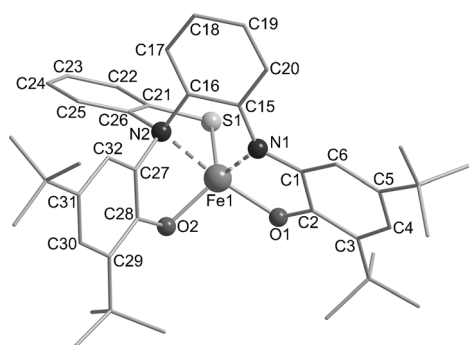


Figure 11. Molecular structure of complex $[L^{SQ}Fe]$ (**6**). Hydrogen atoms are omitted for clarity. Selected bond length [Å] and angles [°]: Fe(1)–O(1) 1.9295(9), Fe(1)–O(2) 1.8929(9), Fe(1)–N(1) 2.0263(12), Fe(1)–N(2) 2.2077(11), Fe(1)–S(1) 2.2683(4), C(1)–C(2) 1.4512(18), C(2)–C(3) 1.4293(18), C(3)–C(4) 1.374(2), C(4)–C(5) 1.429(2), C(5)–C(6) 1.3674(18), C(6)–C(1) 1.4194(19), C(1)–N(1) 1.3500(17), C(2)–O(1) 1.3011(16), N(1)–C(15) 1.3947(17), C(15)–C(16) 1.4156(18), C(16)–C(17) 1.3821(19), C(17)–C(18) 1.395(2), C(18)–C(19) 1.386(2), C(19)–C(20) 1.3839(19), C(20)–C(15) 1.4073(19), C(21)–C(22) 1.402(2), C(22)–C(23) 1.382(2), C(23)–C(24) 1.386(2), C(24)–C(25) 1.386(2), C(25)–C(26) 1.3935(18), C(26)–C(21) 1.3988(19), C(26)–N(2) 1.4711(17), C(27)–N(2) 1.4700(16), N(2)–C(16) 1.4591(16), C(27)–C(32) 1.3763(19), C(32)–C(31) 1.3943(19), C(31)–C(30) 1.394(2), C(30)–C(29) 1.395(2), C(29)–C(28) 1.4108(18), C(28)–O(2) 1.3458(16), O(1)–Fe(1)–S(1) 111.89(3), O(2)–Fe(1)–S(1) 119.08(3), O(1)–Fe(1)–O(2) 104.40(4), O(1)–Fe(1)–N(1) 79.54(4), O(2)–Fe(1)–N(2) 80.21(4), O(1)–Fe(1)–N(2) 155.20(4), O(2)–Fe(1)–N(1) 123.45(4), N(1)–Fe(1)–N(2) 77.79(4).

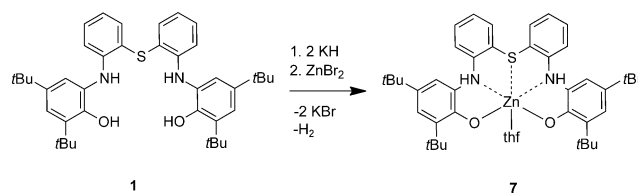
the iron atom is not clear: with a τ factor of 0.53, it lies between the two border cases, square pyramidal ($\tau=0$) and trigonal bipyramidal ($\tau=1$).^[24] Compared to prochiral ligand $[H_2^{Ph2S1}L^{AP}]^{2-}$ of **1**, $[L^{SQ}]^{3-}$ now displays a center of chirality at N(2), and both enantiomers are present in the crystal. With 2.2683(4) Å, the Fe(1)–S(1) bond ranges within Fe–S distances reported for five-coordinate iron(III) complexes.^[25] The observed Fe–O bond lengths, Fe(1)–O(1) 1.9295(9) Å and Fe(1)–O(2) 1.8929(9) Å, compare well to those of **4**. The Fe(1)–N(2) bond is significantly longer [2.2077(11) Å] than the Fe(1)–N(1) bond [2.0263(12) Å], and the coordination sphere around N(1) is trigonal planar ($\Sigma^\circ = 359.7$), thus indicating sp^2 hybridization, whereas the coordination sphere of the N(2) atom is nearly tetrahedral ($\Sigma^\circ = 341.2$).

The C–C bond lengths of the triaryl amino unit are very similar (1.391 ± 0.008 Å), indicating that the conjugation in these aryl rings is retained. With 1.3458(16) Å, the C(28)–O(2) bond obviously shows phenolate anion character. The remaining *tert*-butyl-substituted ring adopts a quinoid-type structure, as evidenced by the typical bond-length pattern of iminobenzo-semiquinone radicals (see above), namely, C(1)–C(2) 1.4512(18), C(2)–C(3) 1.4293(18), C(3)–C(4) 1.374(2), C(4)–C(5) 1.429(2), C(5)–C(6) 1.3674(18), and C(6)–C(1) 1.4194(19) Å. The C(1)–N(2) bond with a length of 1.3500(17) Å is significantly shorter than the C(27)–N(2) bond with a length of 1.4700(16) Å, thus indi-

cating clearly the existence of a C=N bond. Thus, **6** contains a monoradical ligand in its trianionic form, $[L^{SQ}]^{3-}$, and the iron ion can safely be assigned to the +III oxidation state. This is supported by Mössbauer measurements performed on solutions of **5** after exposure to O_2 (\rightarrow **6**); the spectrum showed one quadrupole doublet with $\delta = 0.52 \text{ mm s}^{-1}$ and $\Delta E_Q = 0.89 \text{ mm s}^{-1}$, thus clearly indicating the presence of high-spin Fe^{III} (see the Supporting Information). Compared to the Mössbauer spectrum of **4**, complex **6** shows smaller quadrupole splitting.

Compound **6** derives from **5** through the formal abstraction of the hydrogen atom belonging to the NH unit. Hence, again the above-mentioned hydrogen peroxide test by using the titanil sulfate reagent was carried out (see the Supporting Information). The UV/Vis spectrum recorded after combining the reaction mixture, obtained through treatment of **5** dissolved in THF with O_2 with an acidic aqueous titanil sulfate solution, showed a strong absorption with a maximum at 392 nm, assignable to a $O_2^{2-} \rightarrow Ti$ ligand-to-metal charge transfer, according to the literature.^[15] This points to H_2O_2 formation also in this case, which, however, would require a reaction of HOO radicals, formed in the first bimolecular transformation, with a second equivalent of **5**.

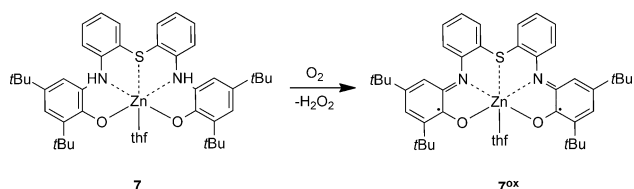
Having found that ligand precursor **1** is stable towards O_2 , while the iron(III) complex **3** reacts, the question arose as to how $[H_2^{Ph2S1}L^{AP}]^{2-}$ would behave after complexation to a redox-inert transition-metal cation, such as Zn^{2+} , which does not possess unpaired electrons and is difficult both to reduce and to oxidize. Treatment of **1** with two equivalents of potassium hydride in dry THF results in the in situ formation of **2**, and addition of $ZnBr_2$ to this yellow solution caused a rapid color change to colorless, thus clearly indicating complexation of Zn^{2+} . After workup, $[H_2^{Ph2S1}L^{AP}Zn(thf)]$ (**7**) was isolated as a colorless solid in 56% yield. The formation of **7** was confirmed by 1H NMR spectroscopy, elemental analysis, IR spectroscopy, and high-resolution ESI mass spectrometry. According to its spectroscopic features, we assume a structural formula for **7** as depicted in Scheme 8.



Scheme 8. Synthesis of $[H_2^{Ph2S1}L^{AP}Zn(thf)]$ (**7**).

Zn^{2+} complex **7** reacts with O_2 to give **7^{ox}**, which is accompanied by a color change to red (Scheme 9). Again, the titanil sulfate test pointed to a simultaneous formation of H_2O_2 , through a strong absorption with a maximum at 400 nm (see the Supporting Information) in the UV/Vis spectrum.

EPR spectra of $[^{Ph2S1}L^{SQ}Zn(thf)]$ (**7^{ox}**) were measured at different fields. In X- and L-band EPR, both spectral patterns and parameters have been found to be similar, thus indicating the ex-



Scheme 9. Synthesis of $[\text{Ph}^{25}\text{L}^{50}\text{Zn}(\text{thf})]$ (7^{ox}).

istence of a hyperfine structure, which is nearly field independent. There is no evidence to suggest strong fine structure. The EPR spectrum of 7^{ox} dissolved in THF at 77 K looks similar to the EPR spectrum of $\text{H}_2\text{Ph}^{25}\text{L}^{\text{OX}}$ (see above). It shows a symmetrical five-line pattern, that can be simulated adequately allowing for hyperfine interactions of a one-electron system to one nitrogen and one hydrogen atom in the immediate vicinity (see Figure 12), which may suggest a localization of the electron at the C atom adjacent to the N atom and a coupling to the nearest ring H atom. However, compared to $\text{H}_2\text{Ph}^{25}\text{L}^{\text{OX}}$, the line width of the signal resulting from 7^{ox} is increased, thus allowing the assumption that redox-inert diamagnetic Zn^{2+} mediates a weak exchange interaction between both radicals.

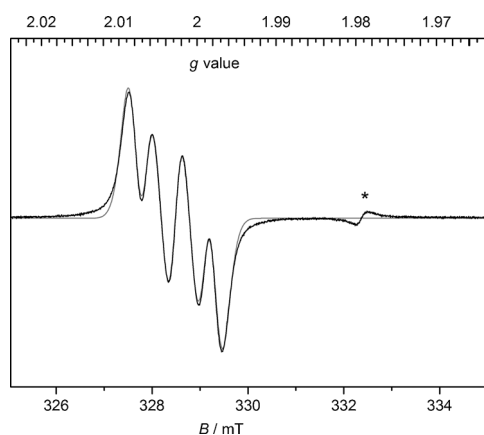
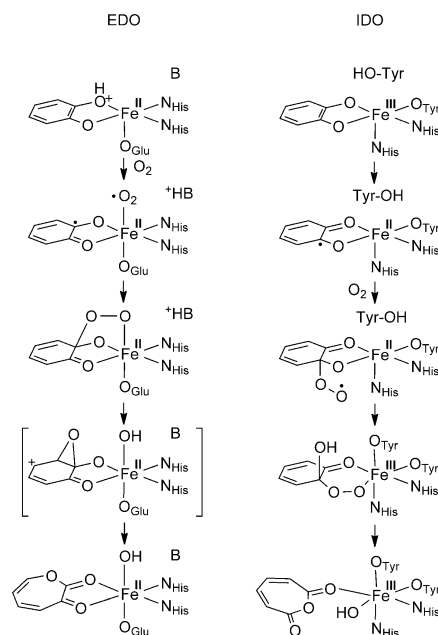


Figure 12. EPR spectrum of complex 7^{ox} dissolved in THF at 77 K directly after its formation through the reaction in Scheme 9. Experimental spectrum shows the $\text{Cr}^{3+}/\text{MgO}$ (*) standard at $g = 1.9796$; the simulated powder spectrum does not show this feature; the g value was determined to be $g' = 2.003$ ($A_{\text{H,atom}}$ 11 MHz coupling to the unpaired electron; $A_{\text{N,atom}}$ 17 MHz coupling to the unpaired electron; spectrometer frequency, 9.246 GHz).

Study of catechol 1,2-dioxygenase activity

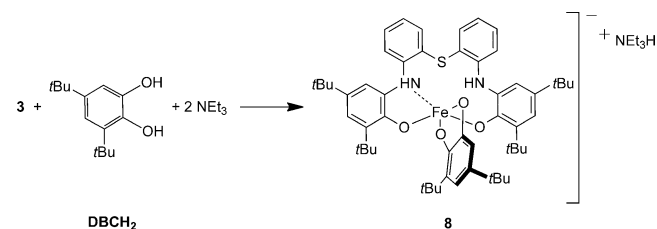
Finally, the iron complexes synthesized were tested with respect to their potential to model catechol dioxygenase reactivity. There are two classes of catechol dioxygenases: the extradiol catechol dioxygenase (EDO) and the intradiol catechol dioxygenase (IDO). The EDO class features an Fe^{II} center in the resting state that activates O_2 to initiate dioxygenation of the substrate; the IDO class contain an Fe^{III} center (coordinated by two tyrosyl and two histidine residues) that activates the catechol substrate by extraction of an electron for the subsequent attack of O_2 . Hence, after binding of the catechol substrate, IDO may be regarded as a Fe^{II} (semiquinone) complex with sub-



Scheme 10. Proposed reaction mechanisms for extradiol catechol dioxygenase (EDO) and intradiol catechol dioxygenase (IDO).^[24]

stantial radical character at the carbonyl C atoms^[26] (Scheme 10).

To examine the catechol-cleaving dioxygenase activity of complex **3**, 3,5-di-*tert*-butylcatechol (H_2DTBC) was chosen as the substrate and employed as follows: the iron complex **3**, H_2DTBC , and NEt_3 in the ratio 1:1:2 were dissolved in THF, leading to a purple-blue solution that presumably contained $[\text{H}_2\text{Ph}^{25}\text{L}^{\text{AP}}\text{FeDTBC}]^-\text{NEt}_3\text{H}^+$ (**8**; Scheme 11).



Scheme 11. Reaction of **3** with 3,5-di-*tert*-butylcatechol and triethylamine.

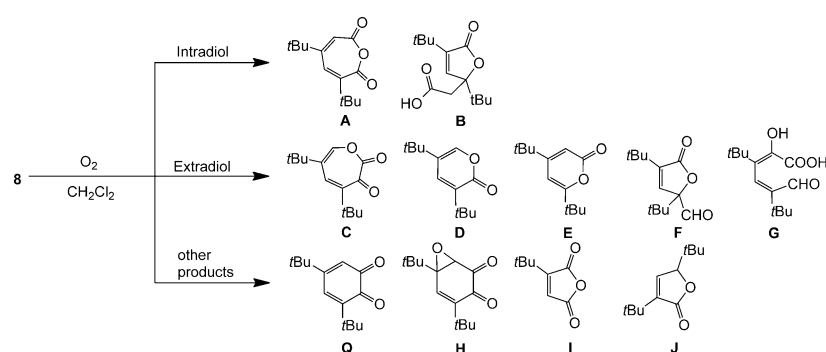
Then, excessive O_2 was added at ambient conditions, leading to an immediate color change to green, and the solution was allowed to stir for 24 h. For an analysis of the reaction products, the reaction was quenched by the addition of 4 M HCl. After workup, the product yields were determined with the aid of ^1H NMR spectroscopy and GC-MS/FID (see Table 1). No attempt was made to separate the products; the isolated mixture of compounds was analyzed to estimate the intra- versus extradiol selectivity. It turned out that under these conditions a multitude of products was formed. 82% of the products could be identified, among them also compounds formed in only small amounts, such as 3,5-di-*tert*-butylfuran-2(5H)-one (**J**; 1% yield). Among the residual 18%, there was no major prod-

Table 1. The time dependence of yields of products of the oxidative cleavage of 3,5-di-*tert*-butylcatechol in the presence of O₂ mediated by complex **3** in THF.

	DTBC	A	B	C	D	E	F	G	H	I	Q
3 h	70%	2%	–	–	7%	4%	–	7%	–	–	7%
6 h	60%	8%	1%	1%	6%	4%	–	9%	3%	–	8%
24 h	0%	9%	–	–	27%	5%	5%	–	9%	9%	17%

uct. Scheme 12 shows the detected products, **A–J**, that are consistent with the products reported in the literature.^[27] The product expected for IDO reactivity would be **A** (3,5-di-*tert*-butyl-1-oxacyclohepta-3,5-dien-2,7-dione) or its hydrolysis product, 3,5-di-*tert*-butyl-5-(carboxymethyl)-2-furanone (**B**). The products generated through the EDO pathway are 4,6-di-*tert*-butyl-1-oxacyclohepta-4,6-diene-2,3-dione (**C**), which is not stable and decomposes to 4,6-di-*tert*-butyl-2-pyrone (**E**) by CO elimination. 3,5-Di-*tert*-butyl-2-pyrone (**D**) is a decomposition product of 5,7-di-*tert*-butyloxepine-2,3-dione, the isomeric EDO cleavage product of **C**. The EDO products, 3,5-di-*tert*-butyl-5-(formyl)-2-furanone (**F**) and *cis,cis*-3,5-di-*tert*-butyl-2-hydroxymuconic semialdehyde (**G**), arise from further intermediates forming during the oxidation reaction.

Fortunately, the yield of quinone **Q**, the most undesirable product, whose formation does not even include an oxygenation but only an autoxidation by two electrons (Scheme 12)



Scheme 12. Products of the oxidative cleavage of 3,5-di-*tert*-butylcatechol by complex **3**.

was comparatively low. As **3** contains Fe^{III} and a quite closed coordination sphere, especially after binding of DTBC²⁻, IDO reactivity was expected. However, the yield of intradiol products, with 9% formation of **A**, was low. After 24 h reaction time, the concentration of extradiol cleavage product **D** (with 27% yield) is the highest and also in sum the yield in EDO products is 4-times higher than the yield in IDO products. This is merely explainable with the availability of a free coordination site at the iron center even after DTBC²⁻ coordination. Although there is a different order of initial events in the intradiol versus extradiol reaction mechanisms, they converge on a common proximal organoperoxide intermediate with iron in the +II oxidation state for EDO and +III for IDO (see Scheme 10). However, it has been suggested, both for the enzymes and their models,

that the choice of intradiol versus extradiol reaction pathways is clearly determined not so much by the iron oxidation states, but rather by stereoelectronic factors influencing the acyl versus alkenyl migration rearrangements of the organoperoxide intermediates.^[28] EDO reactivity requires a binding of the decisive peroxide intermediate to three coordination sites, while IDO requires only two. Therefore theoretical studies were carried out on **8** to find out which donor functions of the ligand may dissociate away from the iron center in the course of 3,5-di-*tert*-butylcatechol binding. In fact, calculations confirmed that after binding of the substrate, the iron center is only five-coordinate and the ligand itself is just coordinating in a tridentate O,N,O fashion (see the Supporting Information). The catechol 1,2-dioxygenase activity of **3** was monitored by UV/Vis absorption spectroscopy (see the Supporting Information). Three new bands emerge at 357 nm ($\epsilon = 12905 \text{ M}^{-1} \text{ cm}^{-1}$), 475 nm ($\epsilon = 3394 \text{ M}^{-1} \text{ cm}^{-1}$) and 767 nm ($\epsilon = 3740 \text{ M}^{-1} \text{ cm}^{-1}$), while an isosbestic point can be observed at 549 nm. We assume that initially, as in case of **3**, hydrogen atoms are abstracted from the NH units, followed by catechol dioxygenation, so that the UV/Vis spectra reflect both events.

Following these ideas further, the solvent is expected to have a pronounced influence on the reactivity. THF, as a solvent with donor properties, can be assumed to coordinate at free iron sites competitively and this, on the basis of the above arguments, could account for the IDO reactivity and **Q** formation observed in parallel. Indeed, changing to the non-coordinating

solvent dichloromethane led to dramatic changes (the yields obtained after 14 h for EDO products **D**, **E**, and **F** are not much lower than those obtained after 24 h, so that only the former are discussed). The yield of **Q** and its autoxidation products are significantly decreased to 9%, extradiol dioxygenase reactivity clearly dominating now (see Table 2). This can be rationalized based on the above hypotheses: the free coordination site at the iron center is now exclusively available to promote EDO cleavage

and this also explains the higher reaction rates (compare Tables 1 and 2). The latter also depend on the electronic properties of the substrate, as shown by the preparation and inves-

Table 2. The time dependence of yields of products of the oxidative cleavage of 3,5-di-*tert*-butylcatechol in the presence of O₂ mediated by complex **3** in dichloromethane.

	DTBC	A	B	C	D	E	F	G	H	I	Q
3 h	16%	3%	2%	10%	20%	6%	2%	–	2%	3%	36%
7 h	10%	3%	4%	–	47%	8%	4%	5%	2%	2%	15%
14 h	0%	7%	2%	–	60%	13%	7%	4%	2%	–	5%
24 h	0%	6%	3%	–	59%	14%	9%	–	1%	3%	5%

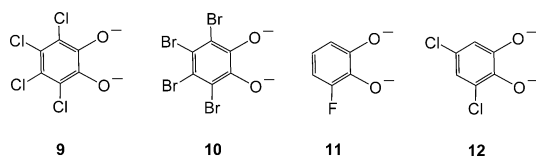
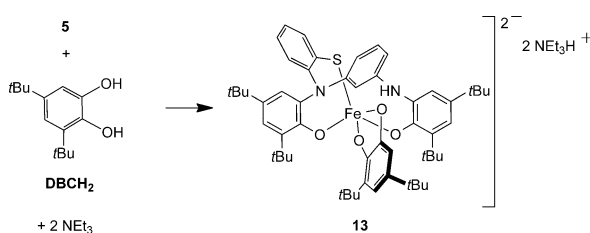


Figure 13. Investigated catecholates with different substituents than in DTBC²⁻.

tigation of analogues of **8** with different substituents at the catecholate (see Figure 13).

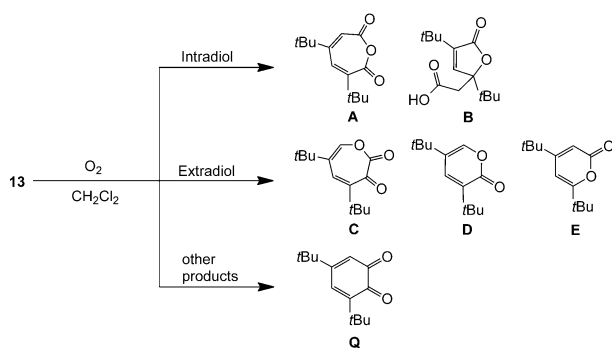
Compounds **9–12**, whose formation could be nicely proved by ESI/MS (see the Supporting Information), behave inert towards O₂. This may be due to the fact that, in the absence of electron-donating groups, the catecholate ligands are not sufficiently electron rich to form iron(II)–semiquinone species for further reaction with O₂.

For comparison, complex **5** was also tested for its catechol 1,2-dioxygenase activity. As before in the case of **3**, **5**, H₂DTBC, and NEt₃ in the ratio 1:1:2 were dissolved in dichloromethane, leading to a purple solution that presumably contained [HL^{AP}FeDTBC]²⁻·2NEt₃H⁺ (**13**; Scheme 13).



Scheme 13. Reaction of **5** with 3,5-di-*tert*-butylcatechol and triethylamine.

Scheme 14 shows the products detected after the reaction with O₂. Obviously, **5** reacts slower, but more selectively than **3** as the number of products, other than those derived from IDO or EDO reactivity, is smaller (Table 3). In addition, extradiol conversion reaches the highest value of 76% after 14 h reaction time and is thus less pronounced than in the case of **3**, while consistently, with 22% yield, the amount of **B** is increased significantly compared to **3**. The fact that only 2% of autoxidation



Scheme 14. Products of the oxidative cleavage of 3,5-di-*tert*-butylcatechol by complex **5**.

Table 3. The time dependence of yields of products of the oxidative cleavage of 3,5-di-*tert*-butylcatechol in the presence of O₂ mediated by complex **5** in dichloromethane.

	DTBC	A	B	C	D	E	Q
3 h	56%	1%	9%	1%	13%	4%	16%
7 h	48%	2%	14%	1%	17%	5%	13%
14 h	–	–	22%	6%	55%	15%	2%

product **Q** is formed and no further side products are formed is remarkable. We thus conclude that, as in case of **3**, two of the donor functions provided by [HL^{AP}]³⁻ dissociate upon catecholate coordination, thus enabling EDO reactivity (see Scheme 10), while the available space is smaller in **13** than it is in **8**, so that IDO cleavage remains competitive.

Conclusion

A novel mixed-donor redox-active ligand, H₄^{Ph₂S₁L^{AP}} (**1**), has been developed and its iron(III) chemistry was explored. Although, after double deprotonation, reaction with FeCl₃ led to a “normal” Cl–Fe³⁺ complex with all five donor atoms of [H₂^{Ph₂S₁L^{AP}]²⁻ coordinated, oxidation of this compound with O₂ led to the formal elimination of H₂ (→H₂O₂) with formation of coordinating iminosemichinone units. Employing Fe[N(SiMe₃)₂]₃ as a precursor for a direct reaction with H₄^{Ph₂S₁L^{AP}}, led to ligand rearrangement through C–S bond cleavage and thiolate formation. Again, the resulting iron(III) complex was susceptible towards oxidation with O₂, leading to a hydrogen atom abstraction and generation of an iminosemiquinone unit. Beyond that, complexes **3** and **5** show interesting properties for applications in bioinspired or biomimetic chemistry, as exemplified here for the case of catechol dioxygenase functioning. The experiments show that **3** and **5** efficiently mediate the oxidative cleavage of 3,5-di-*tert*-butylcatechol with O₂. To understand the role of the metal valency on the selectivity of the C–C bond cleavage, the reactivity of iron(II) catecholate complexes toward O₂ will be studied in future work. The synthesis of iron(II) complexes with this ligand system are currently under investigation.}

Experimental Section

General

All manipulations were carried out in a glove box, or else by means of Schlenk-type techniques involving the use of a dry and O₂-free argon atmosphere. The ¹H and ¹³C NMR spectra were recorded on a Bruker AV 400 NMR spectrometer (¹H, 400.13 MHz; ¹³C, 100.1 MHz) with [D₈]THF as solvent at 20 °C. ¹H and ¹³C chemical shifts are reported in ppm. The ¹H NMR spectra were calibrated against the residual proton, the ¹³C NMR spectra against natural abundance ¹³C resonances of the deuterated solvents. All coupling constants are given in Hz. Solvents were purified employing an MBraun Solvent Purification System SPS. Microanalyses were performed on a HEKAtech Euro EA 3000 elemental analyser. Infrared (IR) spectra were recorded in the region 4000–400 cm⁻¹ by using

solid samples prepared as KBr pellets with a Shimadzu FTIR 8400S. UV/Vis spectra were obtained at variable temperatures on an Agilent 8453 UV-Visible Spectrophotometer equipped with a Unisoku USP-203A cryostat. When necessary, baseline drifting caused by minimal frosting of the cuvettes under low-temperature conditions were corrected by subtracting an average value of a region with no absorbance (1080–1100 nm). Mass spectra (ESI/APCI) were recorded on an Agilent Technologies 6210 Time-of-Flight-LC-MS instrument. X-band and L-Band EPR spectra were recorded on an ERS 300 equipped with a quartz dewar for measurements at liquid nitrogen temperature. The g factors were calculated regarding a $\text{Cr}^{3+}/\text{MgO}$ reference ($g = 1.9796$). Spectral simulations of the EPR spectra were performed using the EasySpin 4.5.1 program. Raman spectra were acquired using a Bruker RAM II FT-Raman Module (1064 nm excitation; Nd:YAG laser). Mössbauer spectra were recorded with a ^{57}Co source in a Rh matrix by using an alternating constant-acceleration Wissel Mössbauer spectrometer operated in the transmission mode and equipped with a Janis closed-cycle helium cryostat. Isomer shifts δ are given in mm s^{-1} relative to iron metal at ambient temperature. The quadrupole splitting ΔE_Q and full width at half maximum values, Γ , are given in mm s^{-1} . Simulation of the experimental data was performed with the Mfit program.^[29]

Materials

Unless otherwise stated, all of the starting materials were obtained at the highest level of purity possible from commercial sources and used as received. Triethylamine was freshly distilled and degassed.

Synthesis and characterization

$\text{H}_4^{\text{Ph}_2\text{S}^{\text{L}^{\text{AP}}}$ (1): To a solution of 2,2'-diaminodiphenyl sulfide (2.48 g, 11.5 mmol) in 75 mL hexane, 3,5-di-*tert*-butylcatechol (5.10 g, 22.9 mmol) and 150 μL (1.1 mmol) triethylamine were added. The resulting suspension was stirred for 18 h, leading to a brown suspension. The hexane solution was decanted from the precipitated solid. The remaining off-white residue was washed twice with 10 mL of hexane and dried in vacuo to give **1** as a white solid (5.24 g, 8.40 mmol, 73%), which was pure according to NMR spectroscopy and elemental analysis. ^1H NMR (400 MHz, $[\text{D}_8]\text{THF}$, 298 K): $\delta = 1.19$ (s, 18H, $\text{C}(\text{CH}_3)_3$), 1.42 (s, 18H, $\text{C}(\text{CH}_3)_3$), 1.73 (m, 4H, THF), 3.58 (m, 4H, THF), 6.47 (dd, $^3J(\text{H},\text{H}) = 8.4$ Hz, $^4J(\text{H},\text{H}) = 1.2$ Hz, 2H, CH), 6.49 (s, 2H, NH), 6.73 (ddd, $^3J(\text{H},\text{H}) = 8.4$ Hz, $^4J(\text{H},\text{H}) = 1.2$ Hz, 2H, CH), 6.81 (d, $^4J(\text{H},\text{H}) = 2.4$ Hz, 2H, CH), 7.06 (ddd, $^3J(\text{H},\text{H}) = 8.4$ Hz, $^4J(\text{H},\text{H}) = 1.2$ Hz, 2H, CH), 7.16 (d, $^4J(\text{H},\text{H}) = 2.4$ Hz, 2H, CH), 7.33 (dd, $^3J(\text{H},\text{H}) = 8.4$ Hz, $^4J(\text{H},\text{H}) = 1.2$ Hz, 2H, CH), 7.34 ppm (s, 1H, OH); ^{13}C NMR (100 MHz, $[\text{D}_8]\text{THF}$, 298 K): $\delta = 29.9$ (CH_3), 31.8 (CH_3), 34.7 ($\text{C}(\text{CH}_3)_3$), 35.6 ($\text{C}(\text{CH}_3)_3$), 114.8 (CH^{Ar}), 119.5 (CH^{Ar}), 119.6 (C), 121.8 (CH^{Ar}), 122.5 (CH^{Ar}), 129.1 (C), 129.7 (CH^{Ar}), 133.7 (CH^{Ar}), 136.4 (C), 142.3 (C), 148.2 (C), 150.4 ppm (C); IR (KBr): $\tilde{\nu} = 3335$ (vs), 3063 (m), 3004 (m), 2957 (vs), 2907 (s), 2867 (s), 1902 (w), 1773 (w), 1773 (w), 1744 (w), 1584 (s), 1474 (vs), 1447 (vs), 1420 (s), 1384 (s), 1365 (s), 1308 (s), 1261 (m), 1229 (vs), 1207 (m), 1154 (m), 1119 (w), 1054 (vw), 1030 (w), 976 (m), 934 (vw), 916 (vw), 879 (w), 853 (vw), 814 (m), 747 (s), 718 (w), 679 (w), 639 (m), 629 (m), 616 (m), 562 (w), 518 (w), 484 (m), 438 cm^{-1} (w); UV/Vis (THF) $\lambda_{\text{max}1}(\epsilon) = 215$ nm ($14716 \text{ M}^{-1} \text{cm}^{-1}$), $\lambda_{\text{max}2}(\epsilon) = 287$ nm ($3717 \text{ M}^{-1} \text{cm}^{-1}$); HRMS (ESI): m/z calcd for $\text{C}_{40}\text{H}_{51}\text{N}_2\text{O}_2\text{S}$: 623.3671 $[\text{M}-\text{H}]^-$; found: 623.3668; elemental analysis calcd (%) for $\text{C}_{40}\text{H}_{52}\text{N}_2\text{O}_2\text{S}$: C 76.88, H 8.39, N 4.48, S 5.13; found: C 77.24, H 8.46, N 4.87, S 4.78; m.p. 236 °C. Crystals of **1** suitable for single crystal analysis were obtained after two weeks from a 1:1 mixture of ace-

tonitrile and dichloromethane by slow evaporation of the solvent mixture.

$[\text{H}_2^{\text{Ph}_2\text{S}^{\text{L}^{\text{AP}}}\text{K}_2(\text{thf})_4$ (2): A THF solution of $\text{H}_4^{\text{Ph}_2\text{S}^{\text{L}^{\text{AP}}}$ (**1**; 2.2 g, 3.520 mmol) was added dropwise to a stirred suspension of KH (310 mg, 7.750 mmol) in 40 mL of tetrahydrofuran at 0 °C over a period of 30 min. The yellow suspension was allowed to warm to room temperature with stirring over 18 h. Filtration, followed by evaporation of the volatiles from the filtrate under reduced pressure, afforded 2.68 g (3.470 mmol, 99%) of **2** as a yellow solid. Diffusion of hexane into a saturated solution of **2** in THF followed by slow evaporation of the volatiles within 2 weeks led to the formation of yellow crystals, which were suitable for single-crystal X-ray diffraction analysis. ^1H NMR (400 MHz, $[\text{D}_8]\text{THF}$, 298 K): $\delta = 1.25$ (s, 18H, $\text{C}(\text{CH}_3)_3$), 1.41 (s, 18H, $\text{C}(\text{CH}_3)_3$), 1.74 (m, 4H, THF), 3.58 (m, 4H, THF), 6.56 (ddd, $^3J(\text{H},\text{H}) = 7.8$ Hz, $^4J(\text{H},\text{H}) = 1.1$ Hz, 2H, CH), 6.75 (d, $^4J(\text{H},\text{H}) = 2.5$ Hz, 2H, CH), 7.07 (ddd, $^3J(\text{H},\text{H}) = 7.8$ Hz, $^4J(\text{H},\text{H}) = 1.1$ Hz, 2H, CH), 7.10 (d, $^4J(\text{H},\text{H}) = 2.5$ Hz, 2H, CH), 7.14 (dd, $^3J(\text{H},\text{H}) = 7.8$ Hz, $^4J(\text{H},\text{H}) = 1.4$ Hz, 2H, CH), 7.42 (dd, $^3J(\text{H},\text{H}) = 7.8$ Hz, $^4J(\text{H},\text{H}) = 1.4$ Hz, 2H, CH), 8.12 ppm (s, 2H, NH); ^{13}C NMR (100 MHz, $[\text{D}_8]\text{THF}$, 298 K): $\delta = 26.2$ (THF), 30.2 (CH_3), 32.5 (CH_3), 34.4 ($\text{C}(\text{CH}_3)_3$), 35.6 ($\text{C}(\text{CH}_3)_3$), 68.0 (THF), 111.7 (CH^{Ar}), 113.3 (CH^{Ar}), 116.5 (CH^{Ar}), 117.6 (CH^{Ar}), 118.3 (C), 129.1 (C), 129.2 (CH^{Ar}), 131.5 (C), 132.9 (CH^{Ar}), 134.1 (C), 146.1 (C), 158.4 ppm (C); IR (KBr): $\tilde{\nu} = 3306$ (w), 3062 (w), 2952 (s), 2903 (m), 2866 (m), 1583 (s), 1565 (m), 1546 (m), 1496 (s), 1472 (s), 1426 (s), 1380 (m), 1358 (m), 1339 (m), 1318 (m), 1280 (m), 1252 (m), 1224 (m), 1200 (m), 1160 (w), 1119 (vw), 1056 (m), 1035 (w), 977 (w), 910 (w), 865 (w), 845 (w), 826 (w), 781 (vw), 746 (s), 672 (vw), 644 (w), 619 (vw), 590 (w), 542 (vw), 512 (w), 441 (vw), 420 cm^{-1} (vw); elemental analysis calcd (%) for $\text{C}_{176}\text{H}_{232}\text{N}_8\text{O}_{12}\text{S}_4\text{K}_8$: C 68.35, H 7.56, N 3.62, S 4.15; found: C 67.89, H 7.47, N 3.62, S 3.63.

$[\text{H}_2^{\text{Ph}_2\text{S}^{\text{L}^{\text{AP}}}\text{FeCl}]$ (3): 100 mg (0.160 mmol) $\text{H}_4^{\text{Ph}_2\text{S}^{\text{L}^{\text{AP}}}$ (**1**) was dissolved in 20 mL THF and treated with 14 mg (0.352 mmol, 2.2 equiv) KH. After 15 min of stirring, 26 mg (0.160 mmol) of FeCl_3 were added, leading to an immediate color change to dark green. After 16 h of stirring at room temperature, the now purple suspension was filtered and the filtrate was reduced to dryness. The resulting black residue was extracted twice with 10 mL hexane, and the solvent was evaporated under reduced pressure. Drying of the residue yielded **3** as a black solid (101 mg, 0.141 mmol, 88%). IR (KBr): $\tilde{\nu} = 3432$ (w), 3369 (w), 3065 (vw), 2958 (vs), 2907 (m), 2869 (m), 1584 (m), 1474 (s), 1452 (m), 1418 (m), 1390 (vw), 1363 (w), 1306 (m), 1260 (m), 1228 (w), 1208 (w), 1161 (vw), 1117 (vw), 1064 (w), 1030 (m), 981 (vw), 913 (w), 873 (w), 832 (w), 809 (w), 750 (m), 668 (w), 594 (w), 543 (w), 492 cm^{-1} (w); UV/Vis (THF) $\lambda_{\text{max}1}(\epsilon) = 287$ nm ($15444 \text{ M}^{-1} \text{cm}^{-1}$), $\lambda_{\text{max}2}(\epsilon) = 470$ nm ($2560 \text{ M}^{-1} \text{cm}^{-1}$), $\lambda_{\text{max}3}(\epsilon) = 844$ nm ($2836 \text{ M}^{-1} \text{cm}^{-1}$); EPR parameter (THF, 77 K): 4.26; elemental analysis calcd (%) for $\text{C}_{40}\text{H}_{50}\text{ClFeN}_2\text{O}_2\text{S}$: C 67.27, H 7.06, N 3.92, S 4.49; found: C 67.36, H 7.16, N 3.64, S 4.20.

$[\text{Ph}_2\text{S}^{\text{L}^{\text{AP}}}\text{FeCl}]$ (4): 50 mg (0.070 mmol) $[\text{H}_2^{\text{Ph}_2\text{S}^{\text{L}^{\text{AP}}}\text{FeCl}]$ (**3**) was dissolved in 5 mL THF and dry O_2 was bubbled through it for 10 s. The reaction mixture turned dark green immediately. After 16 h of stirring, the solvent was evaporated under reduced pressure to yield 34 mg (0.048 mmol, 69%) of **4** as a black solid. IR (KBr): $\tilde{\nu} = 3059$ (w), 2959 (s), 2907 (m), 2869 (m), 1669 (s), 1663 (s), 1609 (w), 1585 (m), 1521 (w), 1467 (s), 1444 (m), 1389 (m), 1364 (m), 1333 (w), 1314 (vw), 1254 (m), 1204 (w), 1178 (vw), 1155 (vw), 1107 (w), 1076 (vw), 1067 (vw), 1025 (m), 994 (w), 964 (vw), 909 (w), 858 (w), 812 (vw), 747 (m), 692 (vw), 670 (vw), 640 (w), 597 (w), 541 (w), 490 (w), 451 cm^{-1} (vw); UV/Vis (THF) $\lambda_{\text{max}1}(\epsilon) = 300$ nm ($17137 \text{ M}^{-1} \text{cm}^{-1}$), $\lambda_{\text{max}2}(\epsilon) = 475$ nm ($2622 \text{ M}^{-1} \text{cm}^{-1}$), $\lambda_{\text{max}3}(\epsilon) = 775$ nm ($3619 \text{ M}^{-1} \text{cm}^{-1}$); HRMS (ESI): m/z calcd for $\text{C}_{40}\text{H}_{48}\text{FeN}_2\text{O}_2\text{S}$: 676.2832 $[\text{M}-\text{Cl}]^-$; found: 676.2680; EPR parameter (low-spin com-

ponent, THF, 77 K): $g_x=2.005$, $g_y=2.061$, $g_z=2.24$. Slow evaporation of a dichloromethane/acetonitrile (1:1) solvent mixture led to the formation of blue-violet crystals of **4** within 10 days; the crystals were suitable for X-ray diffraction analysis.

[HL^{AP}Fe] (5): 86 mg (0.160 mmol) of Fe[N(SiMe₃)₂]₃ was added to a stirred solution of 100 mg (0.160 mmol) H₄^{Ph₂S₁L^{AP}} (**1**) in 20 mL THF. Upon addition, an intensively purple solution was formed. After 16 h of stirring, the solution was evaporated to dryness under reduced pressure to yield 75 mg (0.111 mmol, 69%) of **5** as a purple solid. IR (KBr): $\tilde{\nu}=3629$ (w), 3465 (vw), 3380 (w), 3198 (w), 3060 (w), 2955 (s), 2905 (m), 2868 (m), 1940 (w), 1763 (w), 1582 (m), 1523 (vw), 1474 (s), 1443 (m), 1415 (m), 1388 (m), 1361 (m), 1303 (m), 1254 (m), 1202 (w), 1179 (w), 1111 (w), 1030 (w), 991 (w), 933 (m), 838 (m), 747 (m), 667 (w), 595 (w), 540 (w), 496 (w), 453 cm⁻¹ (vw); UV/Vis (THF): $\lambda_{\text{max}1}$ (ϵ)=286 nm (13304 M⁻¹cm⁻¹), $\lambda_{\text{max}2}$ (ϵ)=328 nm (12234 M⁻¹cm⁻¹), $\lambda_{\text{max}3}$ (ϵ)=560 nm (3280 M⁻¹cm⁻¹), $\lambda_{\text{max}4}$ (ϵ)=892 nm (2878 M⁻¹cm⁻¹); EPR parameter (THF, 77 K): 4.23; elemental analysis calcd (%) for C₄₀H₄₉FeN₂O₂S: C 70.89, H 7.29, N 4.13; found: C 70.35, H 7.20, N 3.93.

[L^{SO}Fe] (6): 50 mg (0.074 mmol) [H₂L^{AP}Fe] (**5**) was dissolved in 10 mL THF and dry O₂ was bubbled through it for 10 s. The reaction mixture turned dark green immediately. After 16 h of stirring, the solvent was evaporated under reduced pressure to yield 37 mg (0.054 mmol, 73%) of **6**. IR (KBr): $\tilde{\nu}=3058$ (w), 2957 (s), 2906 (m), 2869 (m), 1772 (vw), 1674 (m), 1577 (w), 1520 (w), 1466 (s), 1438 (m), 1432 (w), 1385 (m), 1362 (m), 1334 (vw), 1259 (s), 1231 (w), 1178 (w), 1108 (m), 1027 (m), 993 (m), 932 (w), 875 (vw), 838 (m), 819 (m), 805 (m), 745 (m), 669 (w), 645 (vw), 631 (vw), 596 (w), 540 (vw), 490 (w) 450 cm⁻¹ (vw); UV/Vis (THF): $\lambda_{\text{max}1}$ (ϵ)=298 nm (16420 M⁻¹cm⁻¹), $\lambda_{\text{max}2}$ (ϵ)=776 nm (3555 M⁻¹cm⁻¹); HRMS (ESI): m/z calcd for C₄₀H₄₈FeN₂O₂S: 676.2832 [M]⁻; found: 676.2807. Slow evaporation of a dichloromethane/acetonitrile (1:1) solvent mixture led to the formation of black crystals of **6** within 7 days; the crystals were suitable for single-crystal X-ray diffraction analysis.

[H₂^{Ph₂S₁L^{AP}Zn(thf)] (7)}: 100 mg (0.160 mmol) H₄^{Ph₂S₁L^{AP}} (**1**) was dissolved in 20 mL THF and treated with 14 mg (0.352 mmol, 2.2 equiv) KH. After 15 min of stirring, 36 mg (0.160 mmol) ZnBr₂ was added to the yellow solution and the reaction mixture turned colorless immediately. After 16 h of stirring at room temperature, the resulting suspension was filtered and the filtrate was reduced to dryness. Drying of the remaining colorless residue yielded 124 mg (0.181 mmol, 56%) of **7**. ¹H NMR (400 MHz, [D₈]THF, 298 K): $\delta=1.18$ (s, 18H, C(CH₃)₃), 1.45 (s, 18H, C(CH₃)₃), 1.73 (m, 4H, THF), 3.58 (m, 4H, THF), 6.62 (dd, ³J(¹H,¹H)=7.8 Hz, ⁴J(¹H,¹H)=1.2 Hz, 2H, CH), 6.77 (d, ⁴J(¹H,¹H)=2.5 Hz, 2H, CH), 6.88 (t, ³J(¹H,¹H)=7.8 Hz, 2H, CH), 7.08 (d, ⁴J(¹H,¹H)=2.5 Hz, 2H, CH), 7.13 (t, ³J(¹H,¹H)=7.8 Hz, 2H, CH), 7.86 (dd, ³J(¹H,¹H)=7.8 Hz, ⁴J(¹H,¹H)=1.2 Hz, 2H, CH), 7.89 ppm (s, 2H, NH); IR (KBr): $\tilde{\nu}=3300$ (w), 3154 (w), 3068 (w), 2869 (m), 1772 (vw), 1674 (m), 1577 (m), 1520 (w), 1466 (s), 1438 (m), 1432 (w), 1385 (m), 1362 (m), 1334 (vw), 1259 (s), 1231 (w), 1178 (w), 1108 (m), 1027 (m), 993 (m), 932 (w), 875 (vw), 838 (m), 819 (m), 805 (m), 745 (m), 669 (w), 645 (vw), 631 (vw), 596 (w), 540 (vw), 490 (w) 450 cm⁻¹ (vw); HRMS (ESI): m/z calcd for C₄₀H₄₈N₂O₂SZn: 684.2727 [M-2H]⁻; found: 684.2664; elemental analysis calcd (%) for C₄₄H₅₈N₂O₃SZn: C 69.50, H 7.69, N 3.68; found: C 69.71, H 7.42, N 3.73.

Test for H₂O₂ formation^[15]

Several drops of the solutions to be analyzed (e.g., THF solutions of **3** or **5**, after 10 min. of stirring in a dry O₂ atmosphere) were admitted to air and added to a solution of titanil sulfate in water,

which had been acidified with sulfuric acid. After appropriate dilution, UV/Vis spectra were recorded.

Oxidative cleavage of 3,5-di-*tert*-butylcatechol (DBCH₂)

In a typical reaction, 50 mg (0.07 mmol) of **3**, or 47 mg (0.07 mmol) of **5**, respectively, 15.5 mg (0.07 mmol, 1 equiv) DBCH₂ and 20 μ L (0.14 mmol, 2 equiv) NEt₃ were dissolved either in 10 mL THF or dichloromethane under the inert argon atmosphere of a glovebox, and the reaction mixture was stirred for 10 min. Subsequently, excessive O₂ was added and the mixture was stirred for a further 24 h under the O₂ atmosphere. The reaction was quenched by the addition of 20 mL 4 M HCl. Organic products were extracted from the aqueous THF/dichloromethane solution with diethyl ether (2 \times 50 mL), dried over anhydrous MgSO₄, and then concentrated. All volatiles were then removed under vacuum, and the residue was redissolved in CHCl₃. After filtration through silica gel, again all volatiles were removed. The residue was then dissolved in acetonitrile and, after filtration through silica gel, again the solvent was removed under vacuum. The residue was analyzed by ¹H NMR spectroscopy by adding one equivalent of 1,3,5-tribromobenzene to the solution as an internal standard, GC-MS, and GC-FID. Data for 3,5-di-*tert*-butyl-quinone (**Q**): ¹H NMR (CDCl₃, 25 °C): $\delta=1.23$ (s, 9H), 1.28 (s, 9H), 6.22 (d, 1H), 6.93 ppm (d, 1H); HRMS (ESI, MeCN, pos): m/z calcd for C₁₄H₂₀O₂: 220.1463 [M]⁺; found: 220.1822. Data for 3,5-di-*tert*-butyl-1-oxacyclohepta-3,5-diene-2,7-dione (**A**): ¹H NMR (CDCl₃, 25 °C): $\delta=1.17$ (s, 9H), 1.29 (s, 9H), 6.15 (d, 1H), 6.45 ppm (d, 1H); MS (EI, 70 eV): m/z : 236.1 [M]⁺; MS (CI, methanol): m/z : 237.1 [M+H]⁺. Data for 3,5-di-*tert*-butyl-5-(carboxymethyl)-2-furone (**B**): ¹H NMR (CDCl₃, 25 °C): $\delta=0.98$ (s, 9H), 1.24 (s, 9H), 2.91 (d, 1H), 2.81 (d, 1H), 6.92 (s, 1H), 9.72 ppm (s, 1H); MS (EI, 70 eV): m/z : 254.1 [M]⁺; MS (CI, methanol): m/z : 255.1 [M+H]⁺. Data for 4,6-di-*tert*-butyl-1-oxacyclohepta-4,6-diene-2,3-dione (**C**): ¹H NMR (CDCl₃, 25 °C): $\delta=1.15$ (s, 9H), 1.26 (s, 9H), 6.44 (d, 1H), 6.45 ppm (d, 1H); MS (CI, methanol): m/z : 237.1 [M+H]⁺. Data for 3,5-di-*tert*-butyl-2-pyrone (**D**): ¹H NMR (CDCl₃, 25 °C): $\delta=1.22$ (s, 9H), 1.37 (s, 9H), 7.21 (d, 1H), 7.25 ppm (d, 1H); MS (EI, 70 eV): m/z : 208.1 [M]⁺; MS (CI, methanol): m/z : 209.1 [M+H]⁺. Data for 4,6-di-*tert*-butyl-2-pyrone (**E**): ¹H NMR (CDCl₃, 25 °C): $\delta=1.23$ (s, 9H), 1.29 (s, 9H), 6.05 ppm (m, 2H); MS (EI, 70 eV): m/z : 208.1 [M]⁺; MS (CI, methanol): m/z : 209.1 [M+H]⁺. Data for 3,5-di-*tert*-butyl-5-(formyl)-2-furone (**F**): ¹H NMR (CDCl₃, 25 °C): $\delta=1.05$ (s, 9H), 1.25 (s, 9H), 6.90 (s, 1H), 9.60 ppm (s, 1H). Data for *cis,cis*-3,5-di-*tert*-butyl-2-hydroxy-muconic semialdehyde (**G**): ¹H NMR (CDCl₃, 25 °C): $\delta=1.09$ (s, 9H), 1.16 (s, 9H), 5.90 (s, 1H), 9.85 ppm (s, 1H); MS (CI, methanol): m/z : 255.2 [M+H]⁺. Data for 3,4-epoxy-3,4-dihydro-4,6-di-*tert*-butyl-1,2-benzoquinone (**H**): ¹H NMR (CDCl₃, 25 °C): $\delta=1.10$ (s, 9H), 1.20 (s, 9H), 3.80 (d, 1H), 7.07 ppm (d, 1H). Data for 3-*tert*-butylfuran-2,5-dione (**I**): ¹H NMR (CDCl₃, 25 °C): $\delta=1.33$ (s, 9H), 6.52 ppm (s, 1H); MS (EI, 70 eV): m/z : 126.0 [M-CO]⁺, MS (CI, methanol): m/z : 155.0 [M+H]⁺.

Crystallographic studies

All data collections were performed at 100 K on a STOE IPDS 2T diffractometer (Mo-K α radiation, $\lambda=0.71073$ Å, graphite monochromator) area detector. The structures were solved by direct methods (SHELXS-97)^[30] and refined by full-matrix least-squares procedures based on F^2 with all measured reflections (SHELXL-97).^[30] Multi-scan correction (PLATON)^[31] was applied for complex **4**. All non-hydrogen atoms were refined anisotropically. Hydrogen atom positions were either introduced at their idealized positions and were refined by using a riding model or otherwise located in the difference Fourier map. Owing to thermal motion, two *tert*-butyl groups

were found to be disordered over two sites in complex **2**. The 1–2 and 1–3 distances of the disordered parts were restrained to be similar by using the EADP and SADI commands. The restraint EADP was applied to the solvent molecules in **2**.

Crystal data for 1: Empirical formula $C_{40}H_{52}N_2O_2S$; $M_w = 624.90$; orthorhombic; space group $Pccn$; $a = 16.9435(16)$; $b = 22.8430(3)$; $c = 9.2429(9)$ Å; $\alpha = 90$; $\beta = 90$; $\gamma = 90$ °; $V = 3577.4(7)$ Å³; $T = 100$ K; $Z = 4$; 8737 reflections collected, 3300 independent ($R_{int} = 0.1928$), final R indices ($I > 2\sigma(I)$) $R1 = 0.0797$, $wR2 = 0.1966$, R indices (all data) $R1 = 0.1482$, $wR2 = 0.1975$.

Crystal data for 2: Empirical formula $C_{176}H_{232}K_8N_8O_{12}S_4$; $M_w = 3086.69$; triclinic; space group $P\bar{1}$; $a = 15.9835(8)$; $b = 16.9058(9)$; $c = 17.5618(10)$ Å; $\alpha = 72.227(5)$; $\beta = 87.329(5)$; $\gamma = 68.346(4)$ °; $V = 4188.3(4)$ Å³; $T = 100$ K; $Z = 1$; reflections collected, 32321 independent ($R_{int} = 0.1059$), final R indices ($I > 2\sigma(I)$) $R1 = 0.0686$, $wR2 = 0.1593$, R indices (all data) $R1 = 0.1126$, $wR2 = 0.1804$.

Crystal data for 4-(CH₃CN): Empirical formula $C_{42}H_{51}N_3ClFeO_2S$; $M_w = 753.22$; monoclinic; space group $P2_1/c$; $a = 18.1403(10)$; $b = 12.1191(5)$; $c = 18.1756(9)$ Å; $\alpha = 90$; $\beta = 100.332(4)$; $\gamma = 90$ °; $V = 3931.0(3)$ Å³; $T = 100$ K; $Z = 4$; reflections collected, 50615 independent ($R_{int} = 0.0456$), final R indices ($I > 2\sigma(I)$) $R1 = 0.0258$, $wR2 = 0.0650$, R indices (all data) $R1 = 0.0303$, $wR2 = 0.0663$.

Crystal data for 6: Empirical formula $C_{40}H_{48}N_2FeO_2S$; $M_w = 676.71$; monoclinic; space group $P2_1/c$; $a = 14.2319(16)$; $b = 20.4555(14)$; $c = 12.3504(12)$ Å; $\alpha = 90$; $\beta = 91.963(8)$; $\gamma = 90$ °; $V = 3593.3(6)$ Å³; $T = 100$ K; $Z = 4$; reflections collected, 27025 independent ($R_{int} = 0.0281$), final R indices ($I > 2\sigma(I)$) $R1 = 0.0276$, $wR2 = 0.0696$, R indices (all data) $R1 = 0.0316$, $wR2 = 0.0711$.

CCDC 972113 (**1**), 972114 (**2**), 972115 (**4**), 972116 (**6**) contain the supplementary crystallographic data (excluding structure factors) for the structures reported in this paper. These data can be obtained free of charge from the Cambridge Crystallographic Data Centre via www.ccdc.cam.ac.uk/data_request/cif.

Acknowledgements

We are grateful to the Cluster of Excellence “Unifying Concepts in Catalysis” funded by the Deutsche Forschungsgemeinschaft (DFG), and the Humboldt-Universität zu Berlin for financial support. We also want to thank Tobias Spranger for DOSY NMR measurements.

Keywords: coordination chemistry · iron · O–O activation · radicals · redox-active ligands

- [1] a) N. Ito, S. E. V. Phillips, C. Stevens, Z. B. Ogel, M. J. McPherson, J. N. Keen, K. D. S. Yadav, P. F. Knowles, *Nature* **1991**, *350*, 87–90; b) R. M. Wachter, B. P. Branchaud, *J. Am. Chem. Soc.* **1996**, *118*, 2782–2789; c) P. Chaudhuri, M. Hess, U. Flörke, K. Wieghardt, *Angew. Chem.* **1998**, *110*, 2340–2343; *Angew. Chem. Int. Ed.* **1998**, *37*, 2217–2220; d) Y. Wang, J. L. DuBois, B. Hedman, K. O. Hodgson, T. D. Stack, *Science* **1998**, *279*, 537–540; e) C. Wright, A. G. Sykes, *J. Inorg. Biochem.* **2001**, *85*, 237–243.
- [2] A. B. Tomter, G. Zoppellaro, N. H. Andersen, H.-P. Hersleth, M. Hammerstad, Å. K. Röhr, G. K. Sandvik, K. R. Strand, G. E. Nilsson, C. B. Bell III, A.-L. Barra, E. Blasco, L. Le Pape, E. I. Solomon, K. Kristoffer Andersson, *Coord. Chem. Rev.* **2013**, *257*, 3–26.
- [3] a) W. Kaim, B. Schwederski, *Coord. Chem. Rev.* **2010**, *254*, 1580–1588; b) S. Sproules, K. Wieghardt, *Coord. Chem. Rev.* **2011**, *255*, 837–860.
- [4] a) O. R. Luca, R. H. Crabtree, *Chem. Soc. Rev.* **2013**, *42*, 1440–1459; b) P. Chaudhuri, K. Wieghardt, *Prog. Inorg. Chem.* **2001**, *50*, 151–216; c) P. J. Chirik, K. Wieghardt, *Science* **2010**, *327*, 794–795; d) M. M. Allard, J. A. Sonk, M. J. Heeg, B. R. McGarvey, H. B. Schlegel, C. N. Verani, *Angew. Chem.* **2012**, *124*, 3232–3236; *Angew. Chem. Int. Ed.* **2012**, *51*, 3178–3182.
- [5] Review: a) V. K. K. Praneeth, M. R. Ringenberg, T. R. Ward, *Angew. Chem.* **2012**, *124*, 10374–10380; *Angew. Chem. Int. Ed.* **2012**, *51*, 10228–10234; b) P. Chaudhuri, K. Wieghardt, T. Weyhermüller, T. K. Paine, S. Mukherjee, C. Mukherjee, *Biol. Chem.* **2005**, *386*, 1023–1033.
- [6] a) W. Kaim, *Inorg. Chem.* **2011**, *50*, 9752–9765; b) D. Herebian, K. Wieghardt, F. Neese, *J. Am. Chem. Soc.* **2003**, *125*, 10997–11005.
- [7] a) E. Hoppe, C. Limberg, B. Ziemer, *Inorg. Chem.* **2006**, *45*, 8308–8317; b) E. Hoppe, C. Limberg, B. Ziemer, C. Mügge, *J. Mol. Catal. A* **2006**, *251*, 34–40; c) E. Hoppe, C. Limberg, *Chem. Eur. J.* **2007**, *13*, 7006–7016; d) C. Limberg, *Eur. J. Inorg. Chem.* **2007**, 3303–3314.
- [8] R. Metzinger, C. Limberg, *Z. Anorg. Allg. Chem.* **2012**, *638*, 2225–2234.
- [9] M. Costas, M. P. Mehn, M. P. Jensen, L. Que, Jr., *Chem. Rev.* **2004**, *104*, 939–986.
- [10] a) M. T. Gamer, P. W. Roesky, *Inorg. Chem.* **2005**, *44*, 5963–5965; b) C. S. Barrett, *Acta Crystallogr.* **1956**, *9*, 671.
- [11] a) A. J. Bondi, *J. Phys. Chem.* **1964**, *68*, 441–451; b) P. B. Hitchcock, M. F. Lappert, D.-S. Liu, *J. Organomet. Chem.* **1995**, *488*, 241–248; c) P. B. Hitchcock, M. F. Lappert, M. Layh, *J. Chem. Soc. Dalton Trans.* **1998**, 3113–3117.
- [12] S. Pfirrmann, C. Limberg, B. Ziemer, *Dalton Trans.* **2008**, 6689–6691; H. Gehring, R. Metzinger, C. Herwig, J. Intemann, S. Harder, C. Limberg, *Chem. Eur. J.* **2013**, *19*, 1629–1636.
- [13] N. Shaikh, S. Goswami, A. Panja, X.-Y. Wang, S. Gao, R. Butcher, P. Banerjee, *Inorg. Chem.* **2004**, *43*, 5908–5918.
- [14] E. Münck in *Physical Methods in Bioinorganic Chemistry. Spectroscopy and Magnetism* (Ed.: L. Que, Jr.), University Science Books, Sausalito, **2000**, pp. 287–319.
- [15] a) G. M. Maksimov, L. I. Kuznetsova, K. I. Matveev, R. I. Maksimovskaya, *Koord. Khim.* **1985**, *11*, 1353–1357; b) T. Yamase, T. Ozeki, S. Motomura, *Bull. Chem. Soc. Jpn.* **1992**, *65*, 1453–1459.
- [16] a) H. Mimoun, M. Postel, F. Casabianca, J. Fischer, A. Mitschler, *Inorg. Chem.* **1982**, *21*, 1303–1306; b) W. P. Griffith, T. D. Wickins, *J. Chem. Soc. A* **1968**, 397–400; c) A. Butler, M. J. Clague, G. E. Meister, *Chem. Rev.* **1994**, *94*, 625–638.
- [17] a) A. Elmali, Y. Elerman, *Anal. Sci.* **2002**, *18*, 1399; b) A. Elmali, Y. Elerman, *Anal. Sci.* **2001**, *17*, 1137; c) J. A. Bertrand, J. L. Brece, *Inorg. Chim. Acta* **1974**, *8*, 267.
- [18] a) A. Bilyk, J. W. Dunlop, R. O. Fuller, A. K. Hall, J. M. Harrowfield, M. W. Hosseini, G. A. Koutsantonis, I. W. Murray, B. W. Skelton, R. L. Stamps, A. H. White, *Eur. J. Inorg. Chem.* **2010**, 2106–2126; b) C. Desroches, G. Pilet, P. A. Szilagy, G. Molnar, S. A. Borshch, A. Bousseksou, S. Parola, D. Luneau, *Eur. J. Inorg. Chem.* **2006**, 357–365.
- [19] a) M. M. Bittner, D. Kraus, S. V. Lindeman, C. V. Popescu, A. T. Fiedler, *Chem. Eur. J.* **2013**, *19*, 9686–9698; b) A. E. Baum, S. V. Lindeman, A. T. Fiedler, *Chem. Commun.* **2013**, 49, 6531–6533.
- [20] a) H. P. Chun, E. Bill, T. Weyermüller, K. Wieghardt, *Inorg. Chem.* **2003**, *42*, 5612–5620; b) H. Chun, E. Bill, E. Bothe, T. Weyermüller, K. Wieghardt, *Inorg. Chem.* **2002**, *41*, 5091–5099; c) H. Chun, C. N. Verani, P. Chaudhuri, E. Bothe, E. Bill, T. Weyermüller, K. Wieghardt, *Inorg. Chem.* **2001**, *40*, 4157–4166; d) H. Chun, T. Weyermüller, E. Bill, K. Wieghardt, *Angew. Chem.* **2001**, *113*, 2552–2555; *Angew. Chem. Int. Ed.* **2001**, *40*, 2489–2492.
- [21] a) P. Chaudhuri, C. N. Verani, E. Bill, E. Bothe, T. Weyermüller, K. Wieghardt, *J. Am. Chem. Soc.* **2001**, *123*, 2213–2223; b) K. S. Min, T. Weyhermüller, K. Wieghardt, *Dalton Trans.* **2003**, 1126–1132; c) S. M. Carter, A. Sia, M. J. Shaw, A. F. Heyduk, *J. Am. Chem. Soc.* **2008**, *130*, 5838.
- [22] C. Huang, S. Gou, H. Zhu, W. Huang, *Inorg. Chem.* **2007**, *46*, 5537–5543.
- [23] W. M. Singh, B. R. Jali, J. B. Baruah, *J. Chem. Crystallogr.* **2012**, *42*, 775–782.
- [24] A. W. Addison, T. N. Rao, J. Reedijk, J. van Rijn, G. C. Verschoor, *J. Chem. Soc. Dalton Trans.* **1984**, 1349–1356.
- [25] a) E. W. Yemeli Tido, G. O. R. A. van Ekenstein, A. Meetsma, P. J. van Koningsbruggen, *Inorg. Chem.* **2008**, *47*, 143–153; b) C.-M. Lee, C.-H. Hsieh, A. Dutta, G.-H. Lee, W.-F. Liaw, *J. Am. Chem. Soc.* **2003**, *125*, 11492–11493.
- [26] a) T. D. H. Bugg, G. Lin, *Chem. Commun.* **2001**, 941–952; b) S. Mendel, A. Arndt, T. D. H. Bugg, *Biochemistry* **2004**, *43*, 13390–13396; c) T. D. H. Bugg, S. Ramaswamy, *Curr. Opin. Chem. Biol.* **2008**, *12*, 134–140.

- [27] a) M. Ito, L. Que, Jr., *Angew. Chem.* **1997**, *109*, 1401–1403; *Angew. Chem. Int. Ed. Engl.* **1997**, *36*, 1342–1344; b) D. H. Jo, L. Que, Jr., *Angew. Chem.* **2000**, *112*, 4454–4457; *Angew. Chem. Int. Ed.* **2000**, *39*, 4284–4287; c) M. Matsumoto, K. Kuroda, *J. Am. Chem. Soc.* **1982**, *104*, 1433–1434; d) R. Yamahara, S. Ogo, H. Masuda, Y. Watanabe, *J. Inorg. Biochem.* **2002**, *88*, 284–294; e) T. Funabiki, M. Ishikawa, Y. Nagai, J. Yorita, S. Yoshida, *J. Chem. Soc. Chem. Commun.* **1994**, 1951–1952.
- [28] M. Wagner, C. Limberg, T. Tietz, *Chem. Eur. J.* **2009**, *15*, 5567–5576; and references cited therein.
- [29] E. Bill, *Mfit*, Max Planck Institute for Chemical Energy Conversion, Mülheim, Germany.
- [30] G. M. Sheldrick, *Acta Crystallogr. Sect. A* **2008**, *64*, 112–122.
- [31] A. L. Spek, *J. Appl. Crystallogr.* **2003**, *36*, 7–13.

Received: November 19, 2013

Revised: January 15, 2014

Published online on ■ ■ ■■, 0000

FULL PAPER

Ligands

*R. Metzinger, S. Demeshko, C. Limberg****A Novel Pentadentate Redox-Active Ligand and Its Iron(III) Complexes: Electronic Structures and O₂ Reactivity**

A radical convention: A novel pentadentate O,N,S,N,O ligand system, LH₄, which is redox-active, has been developed so that its iron(III) complex (H₂LFeCl) reacts with O₂. H atoms are abstracted from the NH units present so that the ligand is converted into a diradical, featuring two iminosemiquinonato moieties that clamp a high-spin iron(III) center. The complex proved capable of mimicking catechol dioxygenase reactivity, and mediates extradiol cleavage with remarkable selectivity.